Chapter 1

Introduction

The atmosphere is an essential part of life on Earth. The middle and upper regions of the atmosphere are now recognised as important and sensitive indicators of the health of our atmosphere as a whole (e.g., *Roble* [1993]). In particular, the importance of the polar middle atmosphere is now more widely recognised, with changes in occurrence of phenomena such as polar mesospheric summer echoes (PMSEs), polar mesospheric clouds (PMCs) and noctilucent clouds (NLCs) being possible indicators of global climate change [*Thomas*, 1996; *Shettle et al.*, 2002; *Klostermeyer*, 2002]. In spite of this, the polar middle atmosphere remains one of the least understood regions of the Earth's atmosphere.

The Arctic middle atmosphere has been studied using a number of radar, rocket and optical techniques, but there are relatively few such studies in the Antarctic. This thesis uses Medium Frequency (MF) radars located at Davis (69°S, 78°E), Syowa (69°S, 40°E) and Rothera (68°S, 68°W) in the Antarctic, as well as Poker Flat (65°N, 147°W) and Andenes (69°N, 16°E) in the Arctic to study the dynamics of the middle atmosphere in both polar regions.

MF radars can measure wind speeds at heights from about 50 km up to about 100 km. Their continuous operation and relatively good time and height resolutions allow a wide variety of phenomena to be studied including the various types of waves present in the atmosphere. Gravity waves are one type of wave motion which are currently

poorly represented in global climate models (GCMs) [*McLandress*, 1998] and are a focus of this thesis. A greater understanding of gravity waves will be beneficial to GCMs and the climate predictions that they make.

The similar colatitudes of the five MF radars are advantageous for making inter-hemispheric comparisons as is done in this thesis. *Andrews* [1989] notes that there are several areas in which inter-hemispheric comparison of data has scarcely begun, including comparisons of gravity wave characteristics (as measured by radars and lidars, for example), and that there is a clear need for additional data and (perhaps more importantly) more extensive analysis of existing data sets.

The atmospheres of the northern and southern hemispheres show significant hemispheric differences to each other [*Huaman & Balsley*, 1999; *Thomas & Olivero*, 1989; *Andrews*, 1989]. These differences include differences in the average climatological conditions as well as differences in individual events such as major stratospheric warmings.

A major stratospheric warming is a phenomenon that occurs during winter when the stratosphere (the region of the atmosphere between heights of about 10 km and 50 km) suddenly increases in temperature accompanied by a change in direction of the winds (see Section 1.3 for specific details). Major stratospheric warmings occur about once every two years in the northern hemisphere [*Hoffman et al.*, 2002]. However, the first ever observed in the southern hemisphere occurred in 2002, splitting the Antarctic ozone hole apart [*Varotsos*, 2002]. This unprecedented event is investigated in this thesis and compared with northern hemisphere events.

MF radar data were made available from the 5 different locations in the Arctic and Antarctic through international collaborations (see Acknowledgements). Climatologies of the mean winds and gravity waves in the middle atmosphere are investigated, and inter-hemispheric comparisons made. The climatologies are used to investigate the effect that major stratospheric warmings have on the dynamics of the polar middle atmosphere.

This chapter presents background information on topics relevant to this thesis such as gravity waves and stratospheric warmings. A general overview of the atmosphere

as a whole is also presented, with a particular focus on the polar middle atmosphere.

1.1 The Earth's atmosphere

1.1.1 Vertical temperature structure

A convenient method of classifying the Earth's atmosphere is to use its vertical temperature structure. The vertical temperature structure is unlike the vertical pressure structure which decreases in height continuously from the ground up into space. Temperature alternates from the ground upwards between decreasing and increasing layers (see Figure 1.1), giving rise to four distinct regions. These regions in increasing height are termed the troposphere, stratosphere, mesosphere and thermosphere.

The varying shape of the temperature structure is due to the combined effects of solar irradiation, atmospheric dynamics and atmospheric photo-chemistry. Sunlight is absorbed at the surface of the Earth, and then re-emitted at infra-red wavelengths. Water vapour and clouds can absorb some of this infra-red radiation, as can CO_2 and other "greenhouse gases". This causes the "greenhouse effect", where the Earth's surface and the layer of air adjacent to it are 20-30 K higher than the blackbody temperature of the Earth as detected from space. It is this process that causes the temperature distribution of the troposphere, which is the region from the ground up to about 10-15 km. The rate of change of temperature with height is about -6.5 Kkm^{-1} in the troposphere.

The spatial and temporal variation of the surface emission and thermal absorption causes turbulence and convective cells in the troposphere. The negative temperature gradient means that an air parcel that cools adiabatically due to its expansion as it rises can still be warmer than its surroundings. Since the air parcel is warmer than the surrounding air it will continue to rise, leading to a strong mixing of the troposphere due to this convective process.

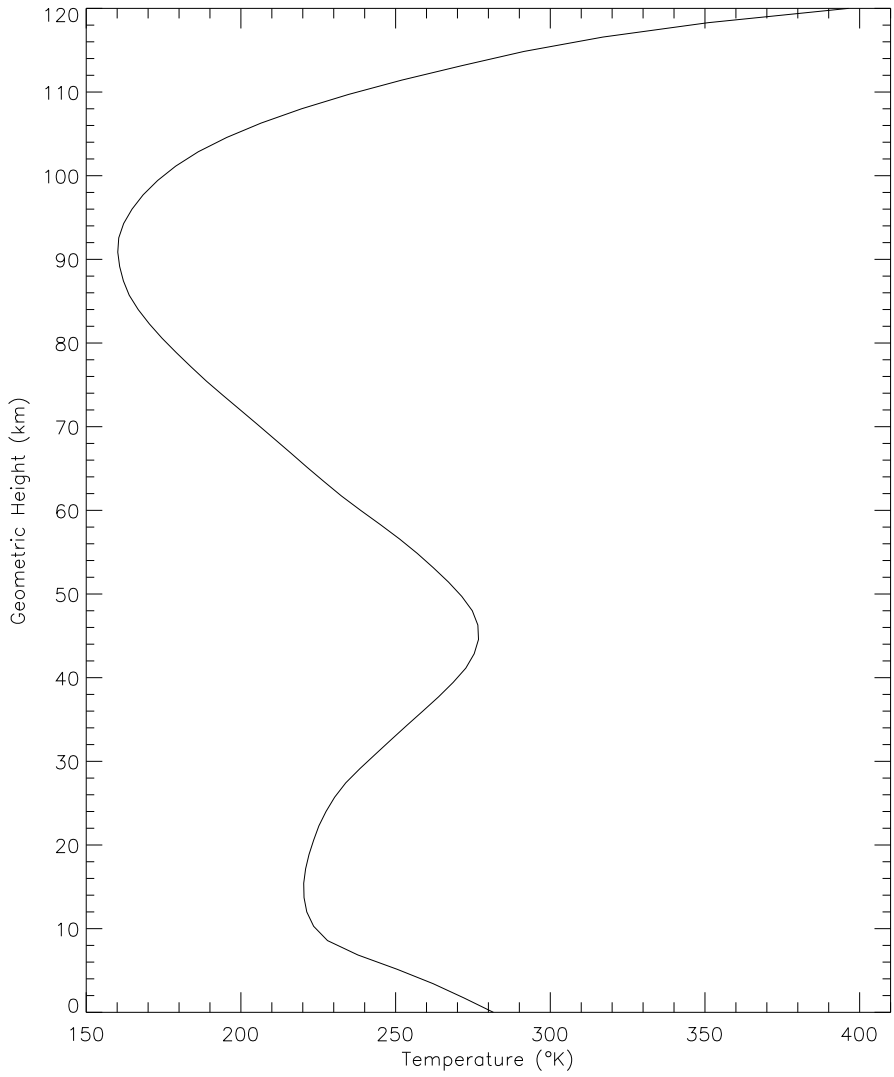

Figure 1.1: Zonal-mean temperature profile from the COSPAR International Reference Atmosphere (CIRA-86) model for January at 50°S.

The upper limit of the troposphere is called the tropopause (meaning turning-level). This is where the stratosphere begins and is defined as the height where the temperature starts to increase with increasing height. This increase in temperature with height is due to the absorption of ultraviolet (UV) solar radiation by ozone [*Park & London*, 1974]. Temperatures range from about 220 K at about 20 km, up to about about 270 K at about 50 km. This positive temperature gradient inhibits convection (this region is mostly mixed by turbulence), resulting in the stratosphere being a very

stable and highly stratified region of the Earth's atmosphere.

The heating which results from the absorption of UV by ozone is greatest at about 50 km, defining the stratopause, above which the mesosphere begins and temperatures start to decrease with height once again. The mesosphere (meaning middle sphere) lies between about 50 km and 90 km. The temperature decreases with increasing height in the mesosphere due to decreasing ozone concentrations with increasing height and the re-radiation of infra-red radiation by CO_2. This decrease in temperature with height continues until the coldest part of the atmosphere is reached at about 90 km, defining the mesopause, where temperatures can fall below 180 K. It should also be noted that the polar winter mesopause occurs significantly higher than this during winter (see Figure 1.2).

Above the mesopause, temperatures start to increase again in the region called the thermosphere which continues out into space. In the thermosphere, photo-absorption by various chemical species leads to a strong increase in temperature with height. The main source of heat in this region is the absorption of extreme UV radiation by atomic oxygen. A large proportion of the air is ionised by the solar extreme UV radiation and X-rays, and so the action of electric and magnetic fields is important for its dynamics.

The mesosphere and lower thermosphere (MLT) is the principal region of interest for this thesis since this is where MF radars obtain neutral wind data.

1.1.2 Global temperature and mean wind climatologies

Figure 1.2 shows contour plots of the zonal (east/west) mean temperature from the CIRA-86 model for January and July [*Fleming et al.*, 1990]. The warmest mean temperatures at the Earth's surface are found in the tropics. At heights near the stratopause a temperature maximum exists at the summer pole. This is consistent with radiative equilibrium expectations due to the maximum in solar ozone heating that occurs here.

There are also features present in Figure 1.2 that cannot be explained by radiative equilibrium alone, such as the local temperature minimum at the tropical tropopause

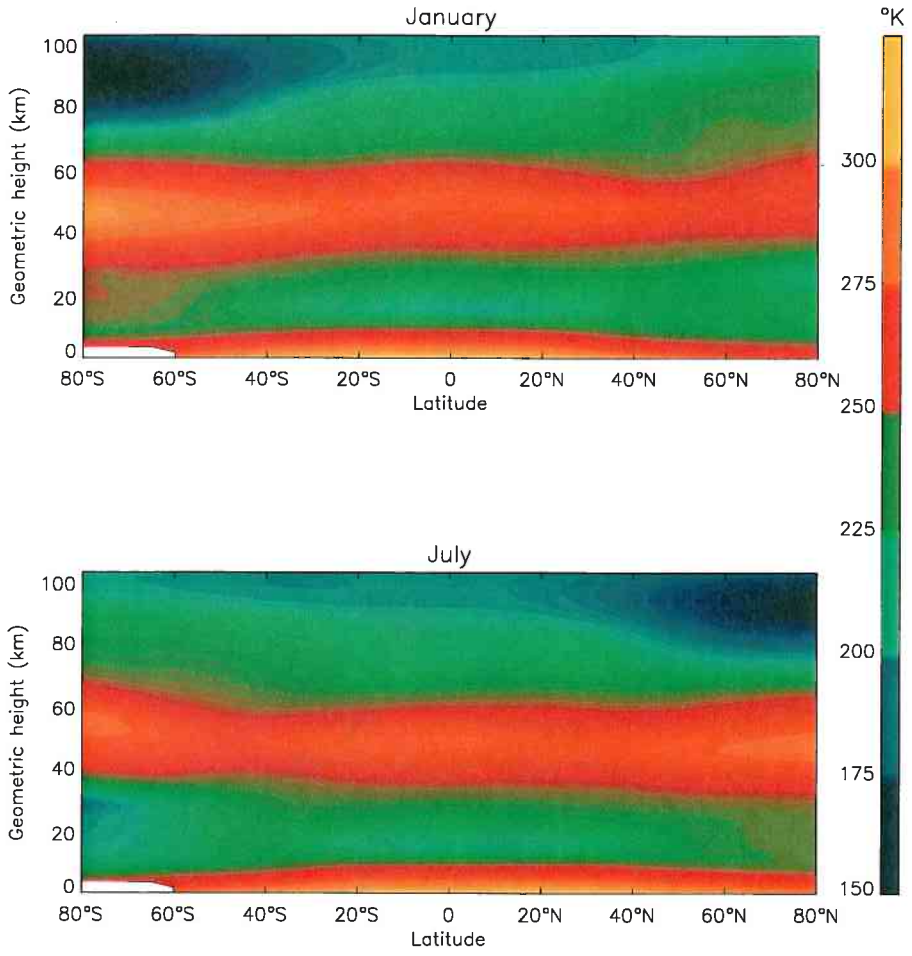

Figure 1.2: Global zonal-mean temperature from the CIRA-86 model shown for January and July.

and the temperature distribution of the mesosphere, with warm temperatures at the winter pole and cold temperatures at the summer pole. These departures from radiative equilibrium are largely due to gravity waves which deposit energy and momentum in the region, changing the dynamics including the meridional flows and forcing the temperatures away from radiative equilibrium conditions (see Section 1.2.5).

Figure 1.3 shows CIRA-86 zonal-mean zonal winds as a function of height and

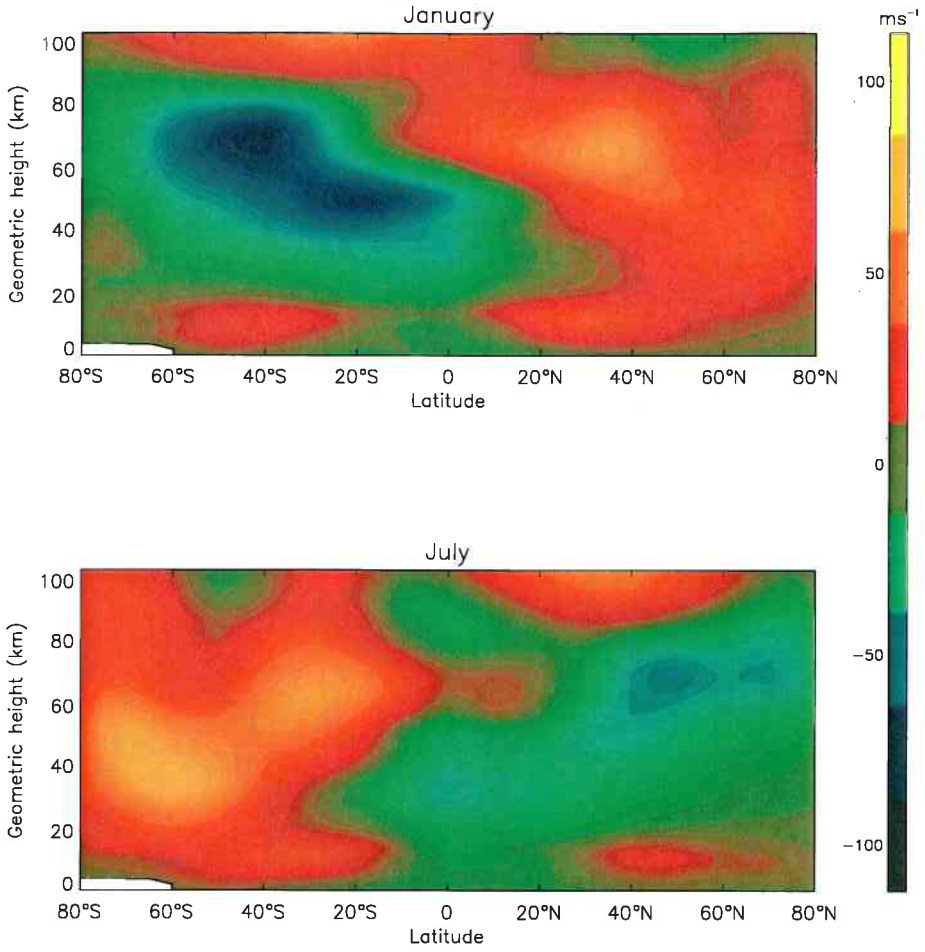

Figure 1.3: Global zonal-mean zonal winds from the CIRA-86 model shown for January and July.

latitude during January and July [*Fleming et al.*, 1990]. The circulation of the stratosphere is normally dominated by a zonally symmetric mean flow that is eastward (positive) in the winter hemisphere and westward (negative) in the summer hemisphere.

1.1.2.1 Polar regions

In polar regions during winter, the absence of sunlight creates an intense cold low pressure system centered approximately over the winter pole. The stratospheric zonal winds during polar winters can become very strong, and are commonly known as the polar night jet or polar vortex.

The cold stratospheric temperatures during the polar winter lead to the formation of polar stratospheric clouds (PSCs) [*Prenni & Tolbert*, 2001] in the Antarctic stratosphere, and also to a lesser extent in the Arctic stratosphere. PSCs are a catalyst in the release of molecular chlorine, Cl_2, from the larger chlorofluorocarbon (CFC) molecules. The formation of these clouds plays a critical role in the destruction of ozone since it is molecular chlorine that reacts with the ozone and not the actual CFC molecules.

The mid-winter stratospheric temperatures inside the polar vortex are an example of where significant differences occur between the northern and southern hemispheres. The winter lower stratosphere is about 20 K cooler in the Antarctic than in the Arctic [*Andrews*, 1989]. The cold temperatures required for PSC formation occur more frequently during the Antarctic winter than during the Arctic winter, leading to a regular hole in the ozone layer over Antarctica (discovered by *Farman et al.* [1985]) during the spring once the solar radiation reaches the clouds and energises the reactions, but only infrequent small amounts of ozone loss in the Arctic.

The coldest part of the Earth's atmosphere is actually the summer polar mesosphere in contrast to what would be expected due to radiative equilibrium conditions alone. Clouds known as polar mesospheric clouds (PMCs) can form in the mesosphere due to the extremely low temperatures which occur there during summer [*Thomas & Olivero*, 1989; *Shettle et al.*, 2002]. PMCs are water ice particles which form as temperatures become less than the frost point for upper mesosphere water vapour concentrations (about $\sim$ 140 K).

Noctilucent clouds (NLCs) are thought to be the visual counterpart of PMCs.

Their name arises because at the height of the mesopause the sun can still be shining on them even though it has set at ground level. The reader is referred to *Gadsden & Schröder* [1989] for a review of NLC research.

Another phenomena which occurs in the polar summer mesosphere are polar mesospheric summer echoes (PMSEs) which are thought to be closely related to PMCs and NLCs and the extremely cold polar summer mesopause temperatures. PMSEs are strong radar echoes from the polar mesosphere during summer that are commonly observed by Very High Frequency (VHF) MST radars. The reader is referred to *Rapp & Lübken* [2004] for a review of PMSE research.

With features such as PMCs, NLCs and PMSEs in the mesosphere, as well as PSCs and the hole in the Antarctic ozone layer in the stratosphere, it is apparent that the polar atmosphere has many unique features. These features result from the polar regions having very distinctive dynamical and temperature structures as compared to other regions of the Earth's atmosphere.

1.2 Gravity waves

1.2.1 Introduction

The motion of the atmosphere, or wind, can be thought of as consisting of a background mean wind, which is a spatial and temporal average, on top of which various wave motions are super-imposed. Gravity (or buoyancy) waves are an important type of atmospheric wave motions, and have a large effect on the middle atmosphere [*Fritts & Alexander*, 2003; *Garcia & Solomon*, 1985; *Luo et al.*, 1995]. Their name arises due to gravity being the restoring force of the oscillation.

Gravity waves were first explained by *Hines* [1960] who suggested they were wave motions in a stratified fluid due to gravity acting downwards and buoyancy acting upwards on vertically displaced fluid parcels. They can be seen as transverse oscillations in the wind perturbations associated with longitudinal oscillations of the temperature,

pressure and density perturbations.

Gravity waves are generally observed to propagate from source regions in the troposphere and stratosphere up into the MLT [*Hirota & Niki*, 1985; *Eckermann & Vincent*, 1989]. To conserve energy, wave amplitudes increase with height since atmospheric pressure decreases with increasing height. The amplitude of the wave motions will continue to increase until it reaches a height where an air parcel's momentum is not reversed in direction by the restoring force of gravity, causing the wave to break. This leads to turbulence and small-scale mixing and is one of the ways in which a wave can become dissipated (see Section 1.2.5 for more details).

At heights in the MLT, gravity wave amplitudes tend to reach this maximum amplitude limit, becoming what is known as "saturated" [*Fritts*, 1989]. At mesospheric heights, gravity wave dissipation drives a mean meridional circulation from the summer to the winter hemisphere. Rising and sinking motions over the poles associated with this meridional circulation lead to strong departures from radiative equilibrium [*Garcia*, 1989; *McIntyre*, 1989], producing the low temperatures required for PMC and NLC formation. An example of this is that the Arctic mesopause is about 60 K colder in summer than in winter [*Lübken & von Zahn*, 1991].

A recent example of the importance of gravity waves was presented by *Gruzdev & Brasseur* [2005] who found that long-term changes in gravity wave activity may contribute significantly to the observed long-term changes in the thermal structure and chemical composition of the mesosphere. Although the effect of gravity waves on the Earth's atmosphere is large, the small spatial scale of individual waves means that their parametrisation is difficult in global climate models due to the large computing power required to resolve them. Research into gravity waves may improve or simplify this parameterisation.

1.2.2 Gravity wave theory

The following theoretical discussion of gravity waves is largely based on *Fritts & Alexander* [2003] and *Andrews et al.* [1987].

1.2.2.1 Static stability

A useful quantity in the description of gravity waves is potential temperature, Θ, defined as the temperature that a parcel of dry air at pressure, p, and temperature, T, would acquire if it were expanded or compressed adiabatically to the reference pressure, p_s:

$$\Theta = T(\frac{p_s}{p})^{\kappa} \tag{1.1}$$

where: $\kappa = \frac{R}{c_p}$ $(\sim \frac{2}{7})$,

with: c_p the specific heat at constant pressure,

and R the gas constant for dry air = 287 $\mathrm{Jkg^{-1}K^{-1}}$.

Unlike temperature, potential temperature is a conserved quantity for adiabatic processes (from the first law of thermodynamics).

Using Equation 1.1, together with the ideal gas law:

$$p = \rho RT \tag{1.2}$$

where: ρ is the density,

and the hydrostatic equation:

$$\frac{\partial p}{\partial z} = -\rho g \tag{1.3}$$

where: z is the geometric height above mean sea level,

and g is the acceleration due to gravity,

yields:

$$T\frac{\partial ln\Theta}{\partial z} = \frac{g}{c_p} - \frac{\partial T}{\partial z} \tag{1.4}$$

Equation 1.4 introduces two terms of importance in gravity wave theory; the lapse rate:

$$-\frac{\partial T}{\partial z}$$

and the adiabatic lapse rate:

$$\frac{g}{c_p}$$

Equation 1.4 shows that the potential temperature will only increase with height when the adiabatic lapse rate is greater than the lapse rate:

$$-\frac{\partial T}{\partial z} < \frac{g}{c_p} \tag{1.5}$$

In this case the atmosphere is said to be statically stable (or stably stratified). In a statically stable region of the atmosphere, any air parcel which undergoes an adiabatic displacement from its equilibrium position vertically upwards (downwards) will be negatively (positively) buoyant.

A parcel of air that is displaced either upwards or downwards will experience a force (due to gravity or buoyancy) that will tend to return it to its equilibrium position. The momentum gained in returning to its equilibrium position will cause the parcel of air to overshoot its equilibrium position and experience a force (due to buoyancy or gravity) in the opposite direction. This process will repeat itself resulting in oscillations of the fluid parcel.

1.2.2.2 Dispersion relation

A derivation of the dispersion relation for gravity wave motions requires the fluid-dynamical equations of motion (e.g., *Holton* [1992]) which are given in Cartesian co-ordinates (x, y, z) by:

$$\frac{du}{dt} - fv + \frac{1}{\rho}\frac{\partial p}{\partial x} = X \tag{1.6}$$

$$\frac{dv}{dt} + fu + \frac{1}{\rho}\frac{\partial p}{\partial y} = Y \tag{1.7}$$

$$\frac{dw}{dt} + g + \frac{1}{\rho}\frac{\partial p}{\partial z} = 0 \tag{1.8}$$

$$\frac{1}{\rho}\frac{d\rho}{dt} + \frac{\partial u}{\partial x} + \frac{\partial v}{\partial y} + \frac{\partial w}{\partial z} = 0 \tag{1.9}$$

$$\frac{d\Theta}{dt} = Q \tag{1.10}$$

where: (u, v, w) is the fluid velocity vector,
X, Y and Q represent unspecified forcings,
and f is the inertial frequency (Coriolis parameter) given by:

$$f = 2\Omega \sin \Phi \tag{1.11}$$

where: Ω is the angular velocity of the Earth,
and Φ is the latitude.

For no forcing (i.e., $X = Y = Q = 0$) and a mean wind given by $(\overline{u}, \overline{v}, 0)$, the following relations can be derived from Equations 1.6-1.10, linearised about a horizontally uniform hydrostatic basic state with $\overline{\Theta}$, $\overline{\rho}$ and $\overline{p}$ varying only in z:

$$\frac{Du'}{Dt} + w'\frac{\partial \overline{u}}{\partial z} - fv' + \frac{\partial}{\partial x}\Big(\frac{p'}{\overline{\rho}}\Big) = 0 \tag{1.12}$$

$$\frac{Dv'}{Dt} + w'\frac{\partial \overline{v}}{\partial z} + fu' + \frac{\partial}{\partial x}\Big(\frac{p'}{\overline{\rho}}\Big) = 0 \tag{1.13}$$

$$\frac{Dw'}{Dt} + g\frac{\rho'}{\overline{\rho}} + \frac{\partial}{\partial z}\Big(\frac{p'}{\overline{\rho}}\Big) - \frac{1}{H}\Big(\frac{p'}{\overline{\rho}}\Big) = 0 \tag{1.14}$$

$$\frac{D}{Dt}\Big(\frac{\Theta'}{\overline{\Theta}}\Big) + \frac{w'N^2}{g} = 0 \tag{1.15}$$

$$\frac{D}{Dt}\Big(\frac{\rho'}{\overline{\rho}}\Big) + \frac{\partial u'}{\partial x} + \frac{\partial v'}{\partial y} + \frac{\partial w'}{\partial z} - \frac{w'}{H} = 0 \tag{1.16}$$

$$\frac{\Theta'}{\overline{\Theta}} = \frac{1}{c_s^2}\Big(\frac{p'}{\overline{\rho}}\Big) - \frac{\rho'}{\overline{\rho}} \tag{1.17}$$

where:

$$H = \frac{RT}{g} \tag{1.18}$$

is the pressure scale height,

$$c_s = \sqrt{\frac{c_p}{c_V} RT_0} \tag{1.19}$$

is the speed of sound with c_V the specific heat at constant volume,

$$\frac{D}{Dt} = \frac{\partial}{\partial t} + \overline{u}\frac{\partial}{\partial x} + \overline{v}\frac{\partial}{\partial y} \tag{1.20}$$

is the linearised form of the time derivative, and

$$N = \Big(g\frac{\partial ln\Theta}{\partial z}\Big)^{\frac{1}{2}} \tag{1.21}$$

is known as the buoyancy frequency (or Brunt-Väisälä frequency) [1].

[1] The buoyancy frequency is a measure of static stability in an atmospheric region as well as being the frequency of the gravity wave oscillations.

We use the WKB approximation which assumes $\overline{u}$, $\overline{v}$ and N vary only slowly over a wave cycle in the vertical (e.g., *Gill* [1982]), neglect background shear and assume wave solutions of the form:

$$(u', v', w', \frac{\Theta}{\overline{\Theta}}, \frac{p'}{\overline{p}}, \frac{\rho'}{\overline{\rho}}) = (\tilde{u}, \tilde{v}, \tilde{w}, \tilde{\Theta}, \tilde{p}, \tilde{\rho}) \bullet exp[i(kx + ly + mz - \omega t) + \frac{z}{2H}] \qquad (1.22)$$

where: (k, l, m) are wavenumbers,
and ω is the ground based wave frequency.

Substituting the wave solutions into Equations 1.12-1.17 and setting the imaginary coefficients to zero gives:

$$\frac{g}{c_s^2} = \frac{1}{H} - \frac{N^2}{g} \qquad (1.23)$$

$$\hat{\omega}^2\Big(k^2 + l^2 + m^2 + \frac{1}{4H^2} - \frac{\hat{\omega}^2 - f^2)}{c_s^2}\Big) = N^2(k^2 + l^2) + f^2(m^2 + \frac{1}{4H^2}) \qquad (1.24)$$

where $\hat{\omega} = \omega - k\overline{u} - l\overline{v}$ is the intrinsic frequency (i.e., the frequency in the reference frame moving with the background mean wind).

Acoustic waves can be removed by letting $c_s \to \infty$, giving the gravity wave dispersion relation:

$$m^2 = \frac{(k^2 + l^2)(N^2 - \hat{\omega}^2)}{(\hat{\omega}^2 - f^2)} - \frac{1}{4H^2} \qquad (1.25)$$

The $-\frac{1}{4H^2}$ term can be neglected for short wavelengths (i.e., $m^2 \gg \frac{1}{4H^2}$). Using this approximation, known as the Boussinesq approximation, and when $\hat{\omega}^2 \gg f^2$, the dispersion relation can be rewritten as such:

$$\hat{\omega}^2 = \frac{N^2(k^2 + l^2)}{k^2 + l^2 + m^2} \qquad (1.26)$$

1.2.3 Gravity wave source mechanisms

Gravity waves will occur when a parcel of air has a different density to the air that surrounds it in a region that is stably stratified. There are a number of different processes that can cause a region of air to have a different density to its surroundings, including wind-orography interaction [*Hines*, 1988], wind shear [*Fritts*, 1982], thunderstorms [*Alexander & Pfister*, 1995], fronts [*Fritts & Nastrom*, 1992], and geostrophic adjustment [*Luo & Fritts*, 1993].

Orographic generation of gravity waves can occur when wind blows over a mountain range. This causes air to be lifted up into a region that is less dense than itself due to the negative vertical gradient of atmospheric density. Gravity wave oscillations will occur as the air parcel tries to return to its equilibrium pressure level if the surrounding atmosphere is stably stratified.

Lenticular clouds are a visual indication of the presence of orographically generated gravity waves. These smooth, cigar shaped clouds are caused by water vapor condensing in the temperature minima of the gravity waves, and can often be seen down wind of mountain ranges.

1.2.4 Turning and critical levels

The vertical wave number, m, must be real (i.e., $0 \leq m^2 \leq \infty$) for vertical propagation of gravity waves. The atmospheric conditions for which m is real can be found from the dispersion relation expressed in terms of the horizontal mean wind, $\overline{u}$:

$$m^2 = \frac{N^2}{(\overline{u} - \hat{c})^2} - k^2 \tag{1.27}$$

where:

$$\hat{c} = c - u(z)cos\phi(z) \tag{1.28}$$

is the intrinsic phase speed with $\phi(z)$ the direction of propagation relative to the mean flow.

The condition $m = 0$ results in what is known as a turning level. Equation 1.27 shows that this will occur if N becomes small due to changes in the temperature with height, or if $(\overline{u} - \hat{c})$ becomes large due to vertical wind shear.

At a turning level a wave will reverse in direction without loss of energy. If multiple turning levels are present at different altitudes the waves can therefore become trapped in a certain height region of the atmosphere. Trapped waves can be ducted between turning levels and propagate over large horizontal distances.

If $\overline{u} - \hat{c} \rightarrow 0$ then $m^2 \rightarrow \infty$, and a process called critical level filtering will occur. In contrast to turning levels, critical level filtering does result in a dissipation of wave energy, with energy and momentum being transferred to the background winds.

Critical level filtering will occur when the intrinsic frequency of a wave is Doppler shifted to zero by the background winds. This results in forbidden phase speeds for each propagation direction, ϕ, (e.g., *Taylor et al.* [1993]) given by:

$$\hat{c} \leq \overline{u}cos\phi + \overline{v}sin\phi \tag{1.29}$$

Gravity waves which reach the mesosphere from source regions at lower heights are therefore expected to have phase speeds outside the range forbidden by the background winds they have encountered.

1.2.5 Momentum deposition

There are a number of dissipative processes that can affect gravity waves. These include wave breaking (convective and dynamic instabilities), turbulent or radiative damping and non-linear wave-wave interactions. Gravity wave dissipation can transport energy and atmospheric constituents from one region of the atmosphere to another, as well as mixing the atmosphere due to the turbulence created by the wave dissipation.

One way that gravity waves can become dissipated is due to the convective instability caused by critical level filtering as discussed in the previous section. Gravity waves can also become convectively unstable when their perturbation amplitude parallel to the direction of horizontal wave propagation, $u'_{||}$, is greater than their intrinsic horizontal phase speed [*Hodges Jr.*, 1967], i.e.:

$$u'_{||} > \hat{c} \tag{1.30}$$

The condition above is important for vertical propagation of gravity waves as their perturbation amplitudes increase to conserve wave energy as pressure decreases with height. When the amplitude becomes too large the waves "break", leading to turbulence, small-scale mixing and wave dissipation.

For waves of periods close to the inertial frequency, f, dynamical instabilities are important [*Dunkerton & Buchart*, 1984; *Fritts & Rastogi*, 1985]. Dynamical instabilities result from the wave-induced vertical wind shear being large enough that the kinetic energy of the wave motion is too large for the restoring force of gravity to reverse the direction of an air parcel's momentum. *Miles* [1961] showed that this will occur when the Richardson number, Ri, is less than $\frac{1}{4}$. The Richardson number is the ratio of the work required to interchange an air parcel with one at an adjacent height, to the kinetic energy available to do the work. The Richardson number is defined as:

$$Ri = \frac{N^2}{(\frac{\partial \overline{u}}{\partial z})^2} \tag{1.31}$$

Another process in which gravity waves can become dissipated is through nonlinear wave-wave interactions. This can occur through either resonant or non-resonant interactions. These processes are discussed by *Dunkerton* [1989] and *Yeh & Liu* [1981].

Gravity wave momentum deposition is commonly accepted to be the cause of the observed mesospheric flow from the summer to winter hemisphere. The non-acceleration theorem suggests that a meridional flow will occur only if wave dissipation

is taking place [*Andrews et al.*, 1987; *Eliassen & Palm*, 1961]. Vertical winds, w, occur to satisfy the required mass continuity resulting in descent in the winter mesosphere, $(\rho w)_z > 0$, and ascent in the summer mesosphere, $(\rho w)_z < 0$.

The adiabatic compression and expansion associated with these vertical motions results in temperature changes as parameterised by *Lindzen* [1981], showing that gravity wave drag and diffusion contributions to the forcing can account for much of the observed departures from radiative equilibrium. The resultant temperature structure is a balance between the radiative effects (known as the "radiative spring") and the dynamical effects caused by wave drag [*Meek et al.*, 1985].

1.3 Sudden stratospheric warmings

1.3.1 Planetary waves and the formation of stratospheric warmings

Sudden stratospheric warmings occur during winter and involve rapid increases in the temperature of the polar stratosphere. They were first discovered by *Scherhag* [1952] from a sudden increase in the radiosonde 10-mbar temperature on January 30 over Berlin.

The sudden warmings are caused by planetary waves, which are zonally traveling wind perturbations of a global scale resulting from the meridional gradient in the Coriolis parameter (i.e., the effect of the Earth's rotation). Planetary waves propagating up from the troposphere can be focused into the stratosphere causing rapid mean-flow changes due to rectified nonlinear effects [*Matsumo*, 1971; *Andrews et al.*, 1987] resulting in sudden stratospheric warmings.

Planetary waves can be classified by the number of complete wave cycles around a circle of longitude at a particular latitude. The number of complete cycles is termed the "zonal wavenumber", which is an integer number, as opposed to the physical wavenumber given by $\frac{2\pi}{\lambda}$ (where λ is the wavelength).

Planetary waves are commonly thought to be generated mostly in the troposphere and stratosphere through processes such as wind-orography interactions and barotropic instabilities in the mean flow. Planetary waves can propagate vertically and have been observed at higher altitudes such as the mesosphere and ionosphere [*Lawrence & Jarvis*, 2001].

Vertical propagation of planetary waves can be prevented by the background winds. *Charney & Drazin* [1961] found that either westward or strong eastward stratospheric winds would trap the waves, preventing them from reaching the mesosphere. Vertical propagation of quasi-stationary planetary waves (i.e., $c \approx 0$) is only possible when:

$$0 < \hat{u} < \frac{\beta}{k^2 + l^2} = u_c \tag{1.32}$$

where: u_c is a critical wind speed,
and $\beta = \frac{\partial f}{\partial y}$ results from the simplification known as the β-plane approximation by setting the Coriolis parameter, f, equal to:

$$f = f_0 + \beta y \tag{1.33}$$

where: $\beta = \frac{\partial f}{\partial y}$ is a constant resulting in a linear relationship between f and latitude, y.

Planetary waves with $c = 0$ will only be able to propagate vertically through weak (depending on scale) positive zonal winds; or if c is not zero, when c is westward relative to the background wind. This condition results in a large difference in planetary wave activity between the winter and summer hemispheres, since the stratospheric zonal winds are generally positive in winter and negative in summer (see Figure 1.3).

1.3.2 Classification of stratospheric warmings

There are a variety of different types of sudden stratospheric warming. Following the classification system of the Stratospheric Research Group of the FU Berlin (e.g., *Labitzke & Naujokat* [2000]), a major stratospheric warming must have a zonal-mean temperature increase poleward from 60 degrees latitude at 10 hPa or below, with an associated circulation reversal poleward of 60 degrees latitude (i.e., net mean easterly winds poleward of 60 degrees latitude). The circulation reversal means that a requirement for a major stratospheric warming is a breakdown or splitting of the winter polar stratospheric vortex.

If the zonal-mean zonal winds at the 10 hPa level do not reverse, but the temperature increases by at least 25 K in a period of a week or less at any stratospheric level in any area of the wintertime hemisphere (as measured by radiosonde or satellite), then the warming is classed as minor.

After some sudden stratospheric warmings the polar stratospheric temperature will decrease and the zonal winds will accelerate eastward returning the stratosphere back to a state typical of winter. However, sometimes a stratospheric warming can lead directly into the change to the summer circulation, with warmer polar stratospheric temperatures and westward zonal winds persisting after the sudden warming event. In this case the warming is classed as a "final warming". Final warmings are common when a sudden stratospheric warming event occurs towards the end of a winter.

Another class of sudden stratospheric warming are termed "Canadian warmings". Canadian warmings are characterised by strong wave-1 amplification in the middle stratosphere resulting in the Arctic vortex shifting off the pole towards Europe (i.e., away from Canada). Canadian warmings rarely lead to a major stratospheric warming (with zonal wind reversals only having been observed six times since regular observations began about 50 years ago [*Manney et al.*, 2001]).

1.3.3 Hemispheric comparisons of stratospheric warmings

A large difference exists between the northern and southern hemispheres in the occurrence of sudden stratospheric warmings. Many major and minor warmings have been observed in the northern hemisphere, with a major warming occurring about once every two northern winters on average [*Labitzke*, 1981; *Schoeberl*, 1978; *Hoffman et al.*, 2002]. In contrast to the northern hemisphere, only one major stratospheric warming has ever been observed in the southern hemisphere in the ∼50 years of regular monitoring that has occurred since the International Geophysical Year (IGY) in 1957. The southern hemisphere major stratospheric warming occurred during September 2002, splitting the Antarctic ozone hole apart [*Baldwin et al.*, 2003; *Varotsos*, 2002].

The hemispheric difference in the prevalence of major stratospheric warmings relates to the fact that planetary waves in the southern hemisphere generally have smaller amplitudes than in the northern hemisphere where orographic and thermal forcing is stronger [*Andrews et al.*, 1987; *van Loon & Jenne*, 1972; *Becker & Schmitz*, 2003]. There was an anomalously large amount of planetary wave forcing in the southern hemisphere during the 2002 winter which weakened and warmed the polar vortex. When the extremely large planetary wave event occurred in September, the stratosphere was already preconditioned to a certain degree for the major warming to occur [*Newman & Nash*, 2005].

It is not known how often major stratospheric warmings occur in the southern hemisphere, but it is known that the 2002 event is unprecedented for at least the last 50 years. With major warmings occurring about once every 2 years in the northern hemisphere it is obvious that a large hemispheric difference exists in the occurrence of major stratospheric warmings.

Significant hemispheric differences also exist in the occurrence of minor stratospheric warmings. Minor warmings are often observed in the southern hemisphere [*Shiotani et al.*, 1993], although they tend to be confined to the middle and upper stratosphere. In the northern hemisphere, it is more typical for minor warmings to

involve the entire stratosphere [*Andrews*, 1989].

An inter-hemispheric comparison of the final warming is given by *Yamakazi* [1987], finding that final warmings in the southern hemisphere are stronger and more rapid than in the northern hemisphere, and that final warmings also differ in their detailed structure and evolution.

The hemispheric differences in the occurrence of sudden stratospheric warmings are related to other hemispheric differences such as the larger amount of PSC formation and ozone loss in the Antarctic stratosphere as compared to the Arctic. A deep minimum in the total ozone column occurs in the Antarctic stratosphere during spring [*Farman et al.*, 1985]. This is in complete contrast to the maximum levels of total ozone which are usually observed during the Arctic spring.

Some Arctic ozone loss due to the presence of PSCs has been observed during particularly cold winter stratospheres (such as those without major stratospheric warmings). However, normally a springtime maximum in ozone occurs in the Arctic, caused by tongues of ozone rich air that move into the Arctic region from lower latitudes at times of breaking planetary waves [*Leovy et al.*, 1985]. The unprecedented Antarctic polar vortex during winter is usually not penetrated by events of this type until after the final warming has occurred [*Dobson*, 1963; *Andrews et al.*, 1987].

The significant hemispheric differences which exist in the occurrence of sudden stratospheric warmings indicate that a high level of independence exists between the northern and southern hemispheres. The southern hemisphere major stratospheric warming therefore provides an opportunity to study major stratospheric warmings from a different perspective.

1.4 Thesis overview

This thesis uses MF radar data from Davis, Syowa and Rothera in the Antarctic, and Poker Flat and Andenes in the Arctic to investigate mean winds and gravity waves in the MLT region. The similar latitudes of the MF radars in the northern and

southern polar regions allow inter-hemispheric climatological comparisons to be made. Mean winds and gravity waves are also investigated during major sudden stratospheric warmings in both hemispheres.

Chapter 2 presents mean wind and gravity wave data obtained from the 5 MF radars. The individual MF radars along with the data analysis techniques that were used are also discussed.

Mean wind climatologies at Davis, Syowa, Poker Flat and Andenes are presented in Chapter 3. Various features present in the climatologies are investigated, such as the timing, height and magnitude of peak wind jets. Hemispheric comparisons of the results are made.

Climatologies of gravity wave activity in the MLT are studied in Chapter 4 using the variances of the MF radar winds. Features such as seasonal variations, spectral content and wave polarisation are investigated. The results are discussed in relation to the mean wind climatologies of the previous chapter.

Chapter 5 presents a summary of all major stratospheric warming events which coincide with the available MF radar data. This includes 6 major warmings in the northern hemisphere, as well as the 2002 southern hemisphere event. The warmings are compared with each other, and classified in terms of properties such as strength and duration.

Chapter 6 details the response of the mean MLT winds to major stratospheric warmings. The mean winds around the time of major stratospheric warmings are investigated, and comparisons are made with the mean wind climatologies of Chapter 3.

The effect that major stratospheric warmings have on gravity wave activity in the MLT is investigated in Chapter 7. The results are compared with the gravity wave climatologies of Chapter 4, and discussed in relation to the effect that major warmings have on the mean winds.

The results of this thesis are summarised in Chapter 8. Conclusions are made, together with suggestions and scope for further work.

Reprints of 3 papers which have already been published as a result of this PhD research are contained in the Appendices. These are:

Appendix G:

Dowdy, A. J., R. A. Vincent, K. Igarashi, Y. Murayama and D. J. Murphy, A comparison of mean winds and gravity wave activity in the northern and southern polar MLT, *Geophysical Research Letters,* **28(8)**, 1475-1478, (2001).

Appendix H:

Kishore P., S. P. Namboothiri, Y. Murayama, R. A. Vincent, A. Dowdy, D. J. Murphy and B. J. Watkins, Further evidence of hemispheric differences in the MLT mean wind climatology: Simultaneous MF radar observations at Poker Flat (65°N,147°W) and Davis (69°S,78°E), *Geophysical Research Letters,* **30(6)**, 10.1029/2002GL016750 (2003).

Appendix I:

Dowdy, A. J., R. A. Vincent, D. J. Murphy, M. Tsutsumi, D. M. Riggin and M. J. Jarvis, The large-scale dynamics of the mesosphere-lower thermosphere during the Southern Hemisphere stratospheric warming of 2002, *Geophysical Research Letters,* **31**, 10.1029/2004GL020282, (2004).

Chapter 2

Data analysis

2.1 Radar techniques

Many different techniques are currently used to study the atmosphere including radars [*Manson et al.*, 1999], lidars [*Senft & Gardner*, 1991], satellites [*Thomas & Olivero*, 1989] balloons [*Allen & Vincent*, 1995] and rockets [*Wu & Widdel*, 1991], each with its own advantages and disadvantages. Ground based remote sensing techniques such as radars ("RAdio Detection And Ranging") and lidars ("LIght Detection And Ranging") have the advantage of continuous measurements with good time and height resolution. These characteristics make them suitable for studying phenomena with the small spatial and temporal scales of gravity wave motions, as is done in this thesis.

The majority of the data used in this thesis was obtained from MF radars. This chapter describes the MF radars and the data acquisition and analysis techniques that were used. It also includes a brief description of work done while in Antarctica as part of this PhD to upgrade the Davis MF radar.

2.1.1 Radar scattering and reflection mechanisms

Radio waves can be backscattered from the atmosphere due to variations of the refractive index of the air [*Gage & Balsley*, 1980]. The refractive index depends on the amount of bound electrons as well as the amount of free electrons in the air. The free

electrons are produced along with positive ions by the ionisation of a number of atmospheric constituents (including molecular oxygen, molecular nitrogen and nitrogen monoxide) by high energy solar radiation and cosmic rays.

The ionosphere is the region of the atmosphere that contains sufficient electron densities that the propagation of radio waves will be affected. A common way of classifying the ionosphere is by the peaks in the vertical profile of electron density. This results in regions, with ascending height termed the D, E, F_1 and F_2 regions [*Rishbeth & Garriot*, 1969]. The D region corresponds approximately with the mesosphere and lies between about 60-90 km. The ionisation in this region is formed mostly by the ionisation of nitric oxide by the solar Lyman-α hydrogen emission line.

The concentration of electrons varies spatially throughout the ionosphere depending on height, season, time of day and other factors such as the amount of solar activity. During the polar winter, when solar ionization is absent, electron precipitation allows radio echoes to occur. The electron concentrations are significantly higher during the day than at night because of the absence of solar radiation at night combined with the recombination of the electrons and positive ions.

The ionosonde was the first form of radar used for atmospheric research. Ionosondes operate by sweeping through a range of frequencies in the high frequency (HF) range of the electromagnetic spectrum. Since different frequencies reflect from different altitudes as the atmospheric electron density changes, a vertical profile of electron densities, known as an ionogram, can be obtained.

Medium frequency (MF) radars operate in the frequency range 1-3 MHz. Radio waves of this frequency are coherently backscattered from sharp gradients in the refractive index caused by turbulence and small-scale wave motion or thin sheets of laminar flow in the D-region of the ionosphere.

Above about 50 km, solar radiation leads to an increase in free electron density with height. Below about 100 km there is a high collision frequency between the ionised particles and the neutral atmosphere causing the ionised particles to be strongly coupled to the motion of the neutral atmosphere. This allows the neutral winds to

be estimated from the partial reflections of the MF radio waves, and is the essence of how MF radars can measure wind speeds.

There are other varieties of atmospheric radars which operate in different frequency ranges. Radars that operate in the very high frequency (VHF) range and the ultra high frequency (UHF) range derive their measurements from weak backscattered signals arising from refractive index fluctuations [*Balsley & Gage*, 1980]. Radars of this variety are commonly known as MST radars because they have height coverage in the mesosphere, stratosphere and troposphere.

2.1.2 Spaced antenna methodology

There are two techniques that are commonly used for continuous radar measurements of the winds in the middle atmosphere. These are the spaced antenna (SA) method [*Mitra*, 1949; *Holdsworth & Reid*, 1995*a*] and the Doppler method [*Hocking et al.*, 1989]. The MF radar data used in this thesis are acquired using the spaced antenna method.

For the spaced antena method, radio wave pulses are transmitted vertically into the atmosphere. Scattering from the atmosphere is measured on the ground where a diffraction pattern of the backscatter is formed. To derive wind speeds, the spaced antenna method requires the diffraction pattern to be measured by at least three spatially separated antennas.

The received signals from each antenna are cross-correlated with each other to calculate the most likely drift speed of the diffraction pattern. The Full Correlation Analysis (FCA) method is commonly used to analyse the raw data in this way to derive the horizontal wind speeds [*Briggs*, 1984].

The spaced antenna method was originally used for total reflection experiments, and then to study partial reflections in the D-region [*Fraser*, 1965; *Briggs*, 1977]. As well as for MF radar wind measurements in the MLT, the spaced antenna method is also currently used for tropospheric and stratospheric measurements using VHF radars if scatter is coherent [*Röttger & Vincent*, 1978], or Incoherent Scatter Radar

(ISR) otherwise.

2.2 The MF radar at Davis, Antarctica

2.2.1 Description

The University of Adelaide in conjunction with the Australian Antarctic Division (AAD) operate a MFSA (Medium Frequency Spaced Antenna) radar located at Davis (69°S, 78°E), Antarctica. It has been operational almost continuously since April 1994. Prior to this, it was operated at Mawson (68°S, 63°E), Antarctica for ∼10 years. In September 1993 it was moved to Davis and upgraded, where operation recommenced with increased effective power and a higher time resolution.

The transmitting array consists of four folded dipoles arranged as a square with sides of 100 m each. The dipoles are suspended at a height of 10 m. The individual transmitting antennas can be phased to allow transmission of clockwise (ordinary-mode or O-mode) or anti-clockwise (extra-ordinary-mode or E-mode) circularly polarised waves. The polar diagram of the transmitting array has a maximum overhead and a null towards the horizon.

It operates at a frequency of 1.94 MHz. Transmission uses pulse widths of 30 μs, which correspond to range resolutions of about 4 km, but are oversampled at 2 km height intervals. Each pulse is a sine wave modulated by a Gaussian envelope. The peak level of the transmitted power is typically about 25 kW (recently upgraded to 40 kW).

The receiver antenna configuration to sample the ground diffraction pattern consists of three crossed dipole antennas, spaced apart from each other in an equilateral triangle with sides of 180 m. Each of the three receiving antennas hangs at a height from 7 m at their centre, to 2 m at their extremities.

The pulse repetition frequency of 80 Hz which is used during summer is the maximum allowable based on the duty cycle of the transmitter. A lower value of 40 Hz

is used during winter since data can be contaminated by range aliasing of strong backscatter from the F-region at heights of about 200-300 km. Multiple pulses are averaged together coherently to improve signal-to-noise ratios such that an averaged sample is stored every 0.4 seconds.

2.2.2 Signal processing

The received signal is amplified and fed into signal processors which sample the voltages. The in-phase and quadrature components of the complex voltages are sampled using an 8-bit (recently upgraded to 12-bit) analogue-to-digital converter to allow it to be sent to the data acquisition PC. The height of an echo is determined using the time delay between the pulse transmission and the returned echo, resulting in a vertical echo profile for each of the three receivers.

The Full Correlation Analysis method is applied to the raw data to determine the horizontal wind speeds. The resultant data will also contain some noise generated from sources including external RF interference and ground clutter. Ground clutter can come from a number of sources including fixed objects such as landforms as well as moving objects such as icebergs or sea scatter in summer due to the horizontal leakage of the transmitted signal. The analysis and display software is capable of removing some of this interference by comparing the power for each spectral bin of the raw data.

To improve the data quality the raw wind data are filtered, with points lying more than 2 standard deviations from the mean value excluded in order to remove outliers. This may cause small amounts of genuine wind data to be rejected, but contamination by external RF interference or poor signal-to-noise is considerably reduced. Although data quality techniques have been applied, some data may still have significant contamination due to ground clutter. A degree of caution should therefore be used in interpreting some data, such as at ranges shorter than about $\sim$70 km during summer due to moving icebergs and sea ice.

Data are taken for 2 minute periods, although whether or not a wind velocity is measured depends on the nature of the scattering irregularities so that the actual time

resolution can exceed 2 minutes. The data acceptance rate for the Davis system is often around 70% at heights near the mesopause.

Signal-to-noise levels define the height range of useful data, so that radars with higher transmitted power should be able to acquire data down to lower heights. The Davis MF radar often acquires useful data down to about 60 km, although this can depend on atmospheric conditions. Conditions such as an abnormally large solar wind flux, known as a polar cap absorption event, cause increased ionisation which can sometimes result in data gaps throughout the MLT region. Another concern is that during summer total reflection may occur at heights below 100 km. The influence of geomagnetic activity on the MLT region at latitudes similar to those of the MF radars has been investigated by *Price et al.* [1991] and is not thought to significantly affect the results presented in this study.

For particle-ionization events geomagnetic latitude is more important than geographic latitude. Geomagnetic latitudes relevant to this study are Davis: 77°S, Syowa: 67°S, Poker Flat: 65°N and Andenes: 67°N. Although Davis and Syowa are relatively close geographically, Davis is typically within the auroral oval whereas Syowa is more typically directly beneath it.

2.2.3 APAC3 upgrade

The Davis MF radar was upgraded in December 2000. The upgrade consisted of a number of improvements, the principal one being to allow the capability to switch between the two circular polarisations that can be used for transmission. The modes correspond to the two possible orientations of circularly polarised waves for quasi-longitudonal propagation along the field lines near the Earth's magnetic poles.

The two different polarisations are created by changing the phasing of the transmitting antennas. The phasing is done by combining a pair of antennas that are at right angles to each other and making them either 90° or 270° out of phase with the other two antennas. The receive antennas can be made to be more sensitive to a particular circular polarisation by phasing them in a similar way to the transmit antennas.

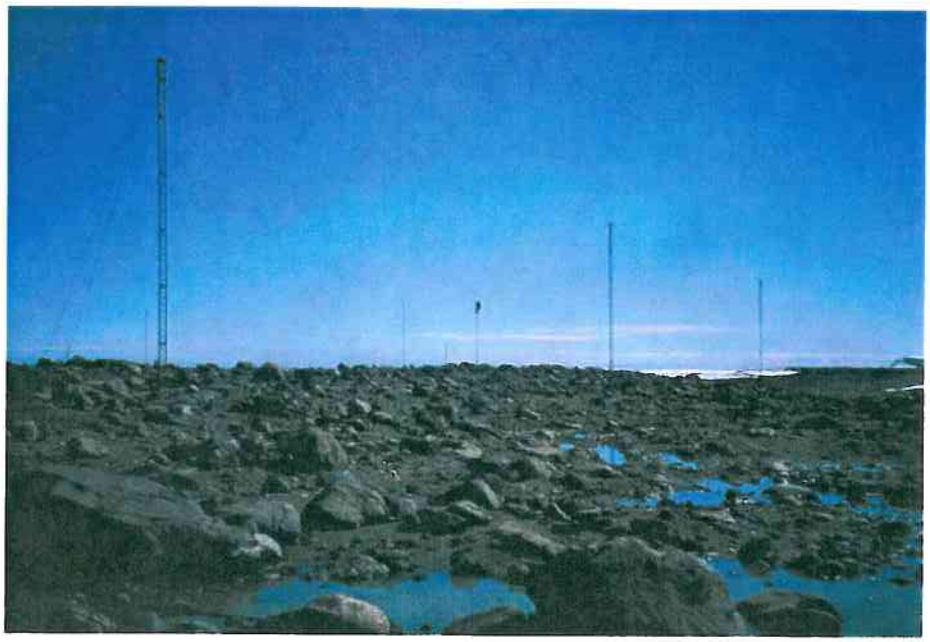

Figure 2.1: The author checking the wiring of a balun box on top of a transmitter tower of the Davis MF radar.

The ability to switch between the two different modes of polarisation is derisable since the MLT has different reflection and transmission coefficients for each polarisation due to the effects of the Earth's geomagnetic field. This property allows electron densities to be measured by determining the amplitude ratio of the E-mode to the O-mode signals. This technique is known as the Differential Absorption Experiment (DAE) [*Gardner & Pawsey*, 1953] and is analogous to a technique which uses the phase difference between the two modes called the Differential Phase Experiment (DPE).

Work was undertaken to modify the wiring on the RF chassis and test the transmission polarisation to allow for the transmission of O-mode and E-mode polarisations. The polarisation testing included climbing the transmitter towers to check the wiring of the balun transformers feeding the transmitter dipoles (see Figure 2.1).

Two new PC's were installed, one for data acquisition and the other for data analysis. This allowed 12-bit data resolution (as compared with the previous 8-bit resolution), remote control and monitoring, IDL-based display and analysis as well as the capabilities to do DAE and DPE experiments.

This thesis focuses on mean winds and gravity waves in the polar MLT. The DAE and DPE capabilities made possible by the upgrade are not a focus of this study. However, the upgrade allows for improved signal-to-noise ratios since switching between the two polarisations allows the optimal polarisation for the prevailing conditions to be selected.

2.3 Available MF radar data

2.3.1 Data overview

Wind data were obtained from 5 MF radars located at Davis, Syowa and Rothera in the Antarctic, and Poker Flat and Andenes in the Arctic. Zonal and meridional winds are shown in Figures 2.1 and 2.2, respectively, for all of the available data. A 14-day running mean is applied to removing the short-term variability, providing an overview of the entire data set.

All 5 MF radars are similar in construction, using the spaced antenna method together with the FCA method to determine horizontal wind speeds in the MLT (e.g., *Murayama et al.* [2000]). They are all similar in operation and data processing and have similar capabilities. The peak transmitted power is one factor that does vary significantly between the radars. The Poker Flat system is somewhat more powerful than the others, resulting in wind measurements down to lower heights on average than the other radars (as can be seen from Figures 2.2 and 2.3).

The similarities that exist between these five radars allow their data to be compared with a high degree of confidence. This conjunction of similar equipment at similar colatitudes is desirable when exploring possible hemispheric differences as is done in this thesis.

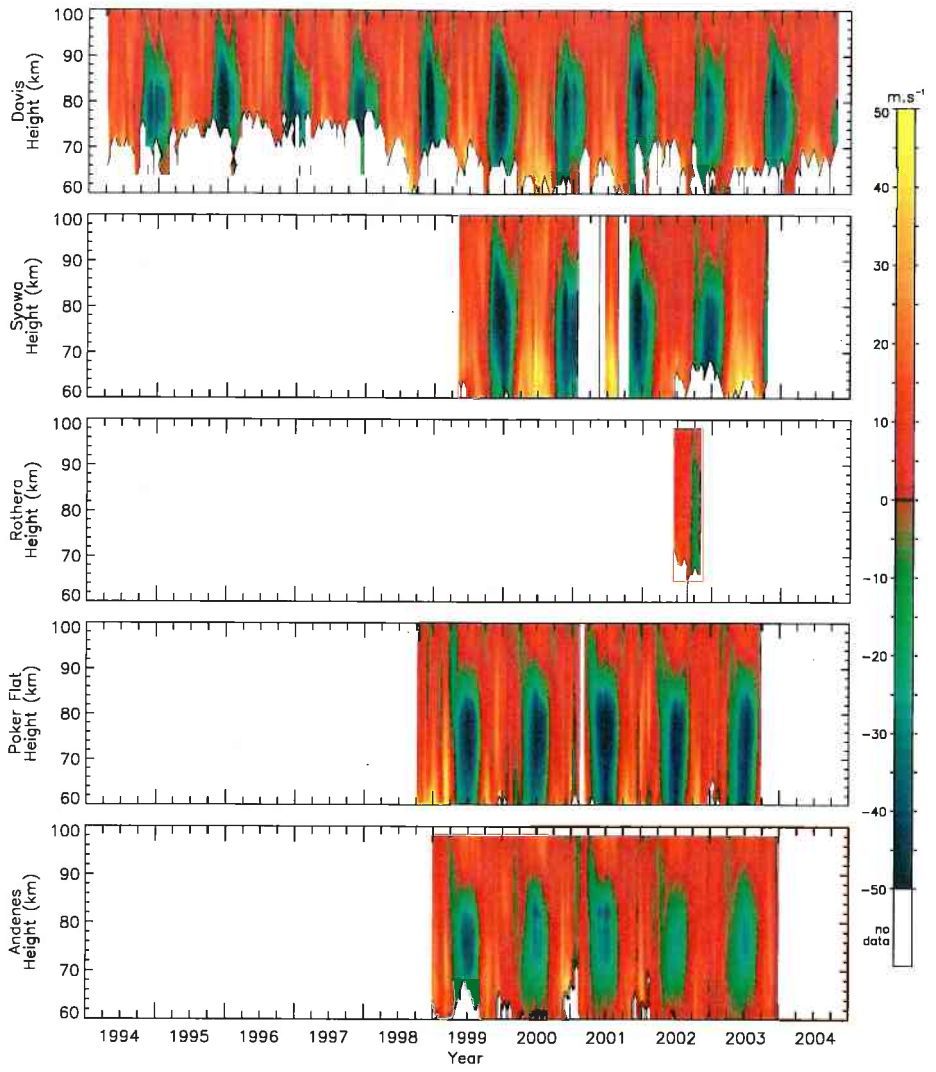

Figure 2.2: MF radar zonal wind data from Davis, Syowa, Rothera, Poker Flat and Andenes. A 14-day running mean is applied.

2.4 Gravity wave analysis

2.4.1 Introduction

There are a variety of methods that can be used to investigate gravity wave activity including wavelet analysis [*Petenko*, 2001; *Torrence & Compo*, 1997], momentum flux measurements [*Wang & Fritts*, 1990; *Alexander & Pfister*, 1995; *Fritts & Yuan*, 1989] or wind variances [*Vincent & Fritts*, 1987] as is done in this study. This section

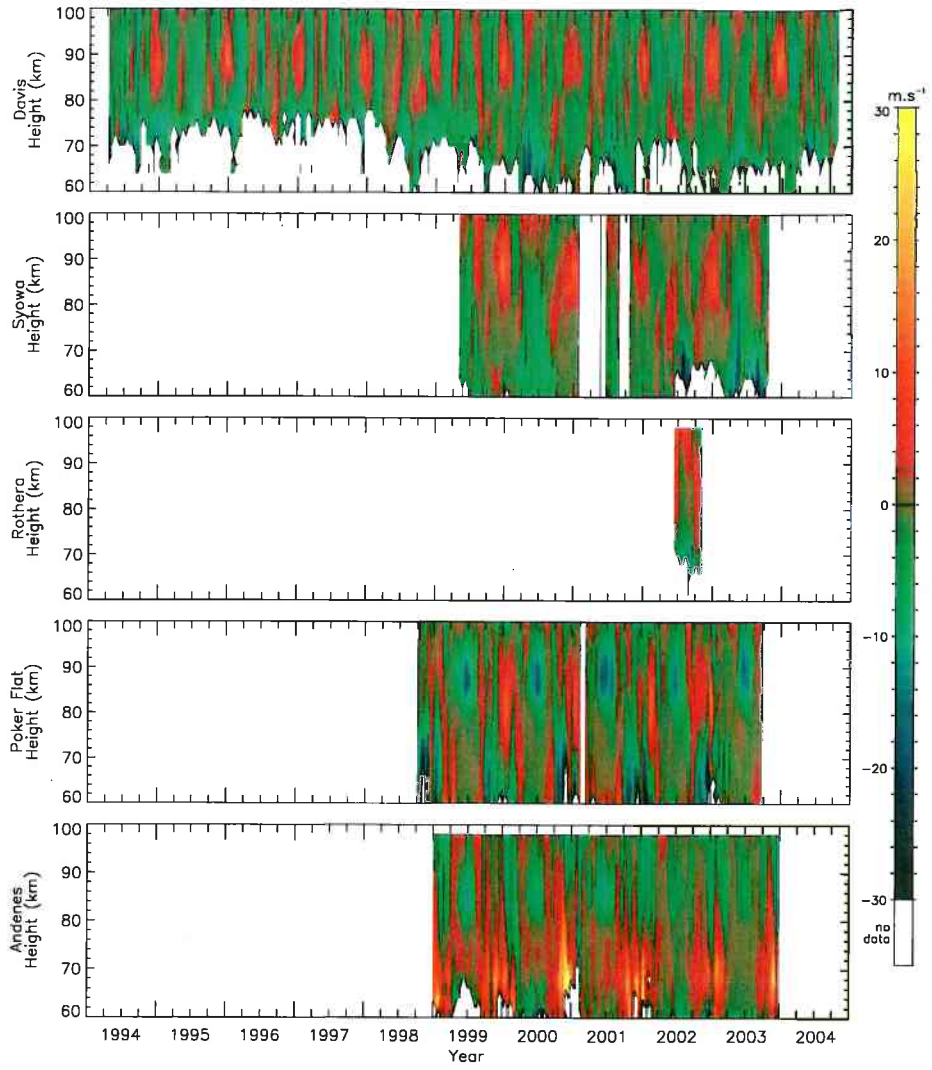

Figure 2.3: As for Figure 2.2, but for the meridional winds.

details the techniques that were used to derive the wind variances for gravity wave investigations in the MLT.

2.4.2 Methodology

The requirement that k, l, and m must all be real in Equation 1.25 for the existence of propagating waves means that:

$$N > \hat{\omega} > f$$

The condition $\hat{\omega} < N$ results from the hydrostatic approximation, and defines the upper limit for gravity wave frequencies. Past this limit the waves cannot propagate vertically and are reflected. At mesospheric heights, this condition restricts gravity wave periods to greater than about 5 minutes, although this value will vary spatially and seasonally.

The condition $\hat{\omega} > f$ shows that gravity wave frequencies must be greater than the inertial frequency (Coriolis parameter) at a particular latitude. At the latitudes of the MF radars used in this study, this limits gravity waves periods to about 13 hours (see Equation 1.11). The reduction in gravity wave activity at the inertial frequency can be seen in Figure 2.4 for the frequency spectra of MF radar winds at Davis and Adelaide (35°S, 138°E) (from *Kovalam & Vincent* [2003]).

The good time resolution of the wind data obtained from MF radars allows gravity wave energy fluxes to be estimated down to relatively short periods. The sampling theorem states that the maximum (Nyquist) frequency which can be represented in a data set is equal to half the sampling frequency of the data. The data have an optimum time resolution of two minutes. However, 10 minute averages are used to reduce the number of data gaps, giving a Nyquist period of 20 minutes.

To reduce the effects of large amplitude 24-hr and 12-hr tides, the time series of each wind component are first harmonically analysed and the resultant tidal harmonic components subtracted from the time series.

Horizontal wind variances are found by computing power spectra of the zonal (u') and meridional (v') perturbation velocities. The power spectra are calculated using Fast Fourier Transform (FFT) methods. The zonal wind variances, $\overline{u'^2}$, and the meridional wind variances, $\overline{v'^2}$, in a particular period range are then measured by integrating the power spectrum over the desired period range.

There are some difficulties that need to be addressed when this methodology is put into practice. These difficulties, and the techniques used to overcome them, are detailed in the following sections.

2.4.3 Data windowing

Leakage is the name given to a problem associated with using Fourier methods on data sets of finite length. A finite length data set is equivalent to multiplying an infinitely long data set by a rectangular function equal to unity during the finite length of data and zero at other times. This effective multiplication of the data by a rectangular function produces the convolution of their Fourier transforms in the frequency domain. The resultant power spectra will therefore contain erroneous frequencies, known as leakage.

One way of reducing leakage is to multiply the original data by a function that changes from zero to one and then back again to zero in a more gradual way than a step function. These so called "window functions" have the effect of smoothing the edges of the original data.

Commonly used window functions include the Hann Window, the Hamming window, the Bartlett window and the Welch window [*Press et al.*, 1992]. The gravity wave analysis presented here uses a Welch window which is a parabola that falls to zero at the edges and is equal to unity in the middle. It is widely used for data with low signal-to-noise ratios. The Welch window function, $W(j)$, is given by:

$$W(j) = 1 - \left(\frac{j - \frac{n}{2}}{\frac{n}{2}}\right)^2 \tag{2.1}$$

where: j is the dependent time variable during the sampling period
and n is the number of data points

Window functions cause an effective reduction in the number of points that contribute to the power spectrum as points multiplied by small values of $W(j)$ only contribute a little to the power spectrum. This will broaden the frequency resolution of the power spectrum due to the sampling theorem, which in turn reduces the variance

of the power spectrum. The effective reduction in the number of points also causes the variance of the power spectrum to increase, so these two effects work on the variance in opposite directions and their effects compensate.

It is possible to recover the information from points at the extremes of the Welch window that do not contribute much to the power spectrum. The information can be fully recovered by using a technique which splits the data set into small overlapping segments so that each data point will be near the middle of the window function in one of the segments [*Welch*, 1967]. Power spectra are then computed for each individual segment. The individual power spectra are then averaged for the time period required to produce an average power spectrum.

2.4.4 Filtering

There is a universality in the gravity wave power spectra observed in the Earth's atmosphere [*VanZandt*, 1982]. The observed power spectra tend to have a slope of about $f^{\frac{5}{3}}$, where f is the ground based frequency of the waves, regardless of season, location or altitude. Power spectra of this shape are commonly described as a red noise spectrum.

Typical power spectrums obtained while calculating the wind variances for gravity wave investigations are shown in Figure 2.5. At low frequencies the spectra have a slope of approximately $f^{\frac{5}{3}}$. At higher frequencies the spectra flatten due to the effects of noise from unwanted influences such as external RF interference and uncertainties in the wind measurements. This is known as a white noise floor as it consists of a constant average power at all frequencies.

A common way to remove a white noise source is a process called Weiner filtering [*Press et al.*, 1992]. It is performed by subtracting a constant value noise floor from the power spectrum at all frequencies to improve signal-to-noise levels. Its effect is most significant at the high frequency end of the spectrum where the signal levels are relatively low.

The noise floor level can be seen in Figure 2.5 to be about $2\text{x}10^4$ $\text{m}^2\text{s}^{-2}\text{Hz}^{-1}$ for

both the zonal and meridional components of the power spectrum. This noise floor corresponds to an uncertainty in wind speed of $\sim$4 ms^{-1} when integrated in frequency up to 8x10^{-4} Hz (a period of $\sim$20 minutes).

Different MF radars will have different noise floors due to their individual locations. Weiner filtering with different noise floors for each radar is used to minimise the effect of noise at each location.

2.4.5 Gravity wave data

The data made available from Davis, Syowa, Poker Flat and Andenes were all in FCA format (2 minute resolution data with errors determined from the FCA method), suitable for the gravity wave analysis. The data from Rothera made available for this study consisted of ASCII wind speed data without the standard error values for each measurement which are used for the calculation of the gravity wave variances. This meant that the Rothera data were not suitable for the gravity wave analysis undertaken in this study, but were suitable for calculating daily averaged wind speeds. Rothera data were only available for about 4 months in total around the time of the 2002 southern hemisphere major stratospheric warming.

Wind variances were calculated at Davis, Syowa, Poker Flat and Andenes. This was done in both the zonal and meridional directions seperately to allow anisotropic investigations to be made. The spectra were integrated in two different period ranges, 20-120 minutes and 120-480 minutes, to provide some information on spectral content.

The variance calculations are restricted to periods less than 8 hours because motions due to transient polar normal modes or intra-diurnal modes with periods in the range 8-12 hr are a significant feature of the wind field at these latitudes [*Forbes et al.*, 1999; *Kovalam & Vincent*, 2003]. The lower height range is restricted to 70 km due to the low availability of data beneath this height.

Gravity wave variances for Davis, Syowa, Poker Flat and Andenes are shown in Figures 2.6 and 2.7 for the zonal and meridional variances, respectively, in the period range 20-120 minutes. A 14-day running mean is applied, removing the short-period

variability so as to provide an overview of the entire data set. Figures 2.8 and 2.9 are similar to Figures 2.6 and 2.7, respectively, but for the period range 120-480 minutes.

The gravity wave data presented here are investigated in detail in later chapters. Gravity wave climatologies are investigated in Chapter 4, and the effect of major stratospheric warmings on gravity wave activity in the MLT is investigated in Chapter 7.

2.5 Summary

The general principles of atmospheric MF radars were discussed in this chapter. Data analysis techniques were detailed for deriving the mean winds from MF radar observations. The total amount of zonal and meridional wind data from the 5 MF radars used in this study were presented. The available periods of wind data consist of about 10 years from Davis, 5 years from Syowa and 4 months from Rothera in the Antarctic, together with about 5 years from both Poker Flat and Andenes in the Arctic.

The methods used to produce wind variance data for gravity wave analysis were detailed. Wind variances at Davis, Syowa, Poker Flat and Andenes were presented for all available years of data. Variances were shown for both the zonal and meridional wind directions in the period ranges 20-120 minutes and 120-480 minutes.

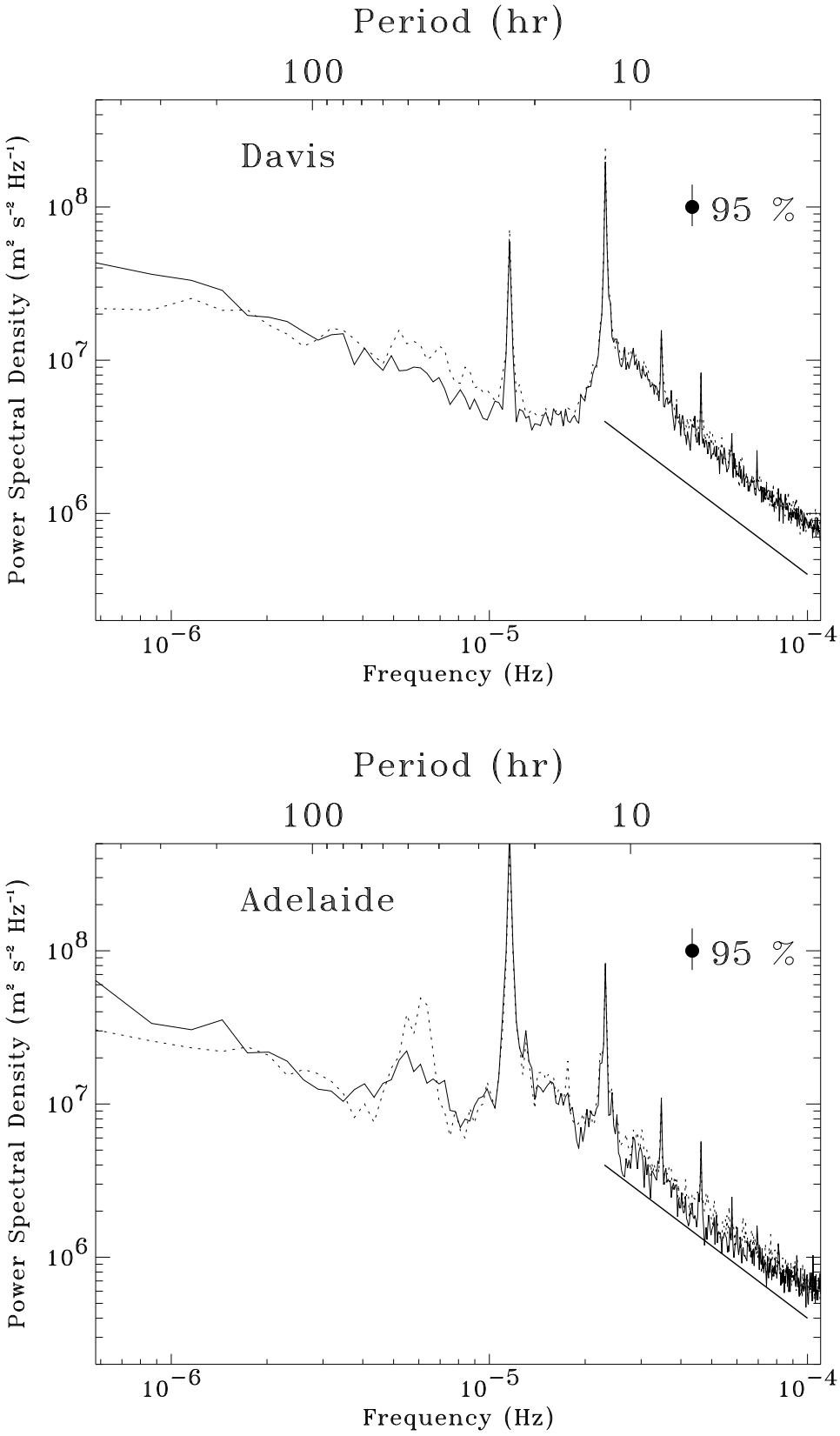

Figure 2.4: Frequency spectra of hourly averaged MF radar winds at Davis and Adelaide (from *Kovalam and Vincent*, 2003). Winds are averaged between 86 and 92 km. The solid lines correspond to zonal winds and the dotted lines correspond to meridional winds. The straight lines have a slope of 5/3 for reference purposes.

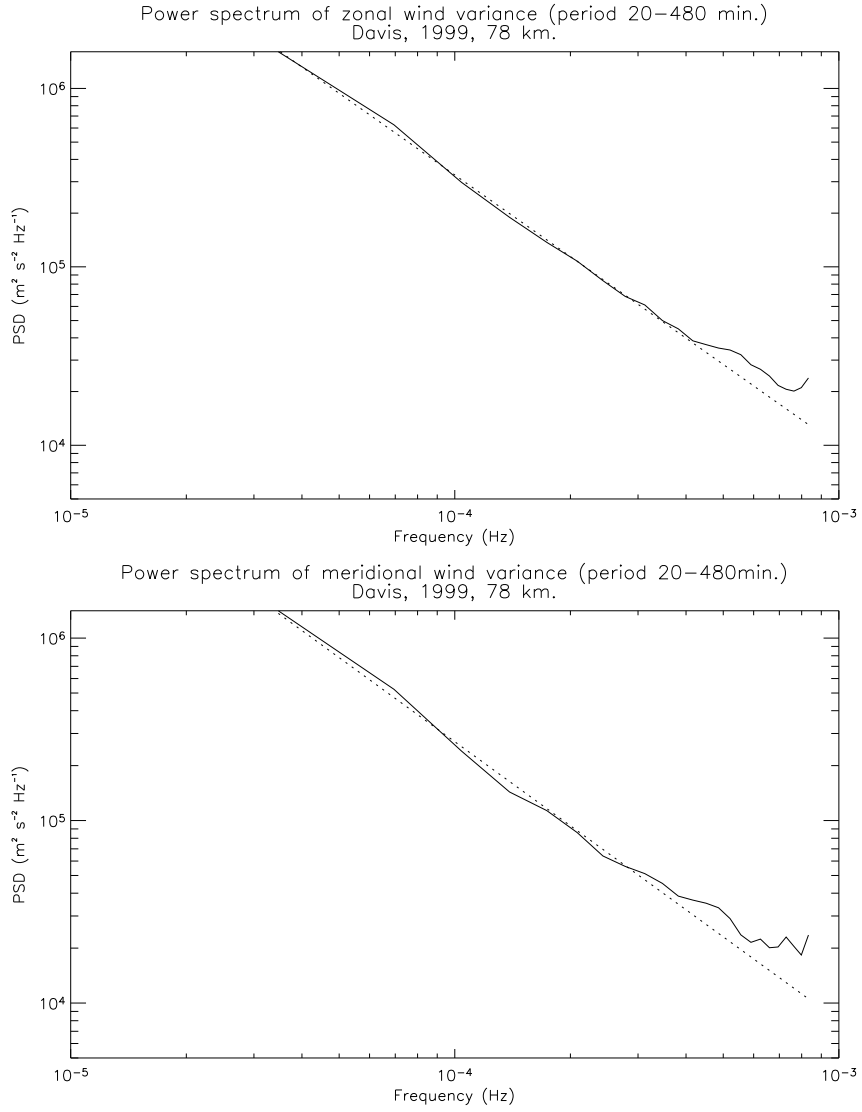

Figure 2.5: A typical power spectrum of the horizontal wind variances obtained for gravity wave investigations. This power spectrum was produced using winds at a height of 78 km from the Davis MF radar on the 10th and 11th of March 1999.

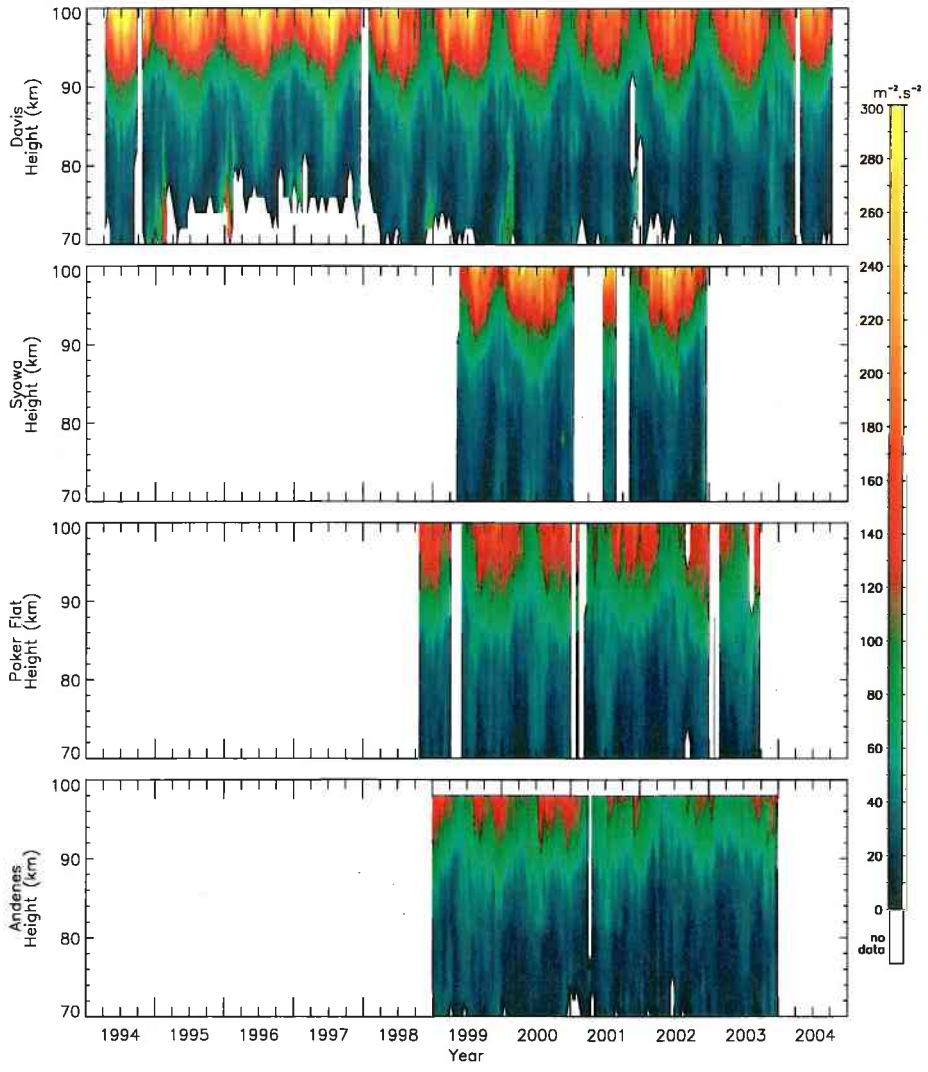

Figure 2.6: Zonal wind variances from Davis, Syowa, Poker Flat and Andenes in the period range 20-120 minutes. A 14-day running mean is applied.

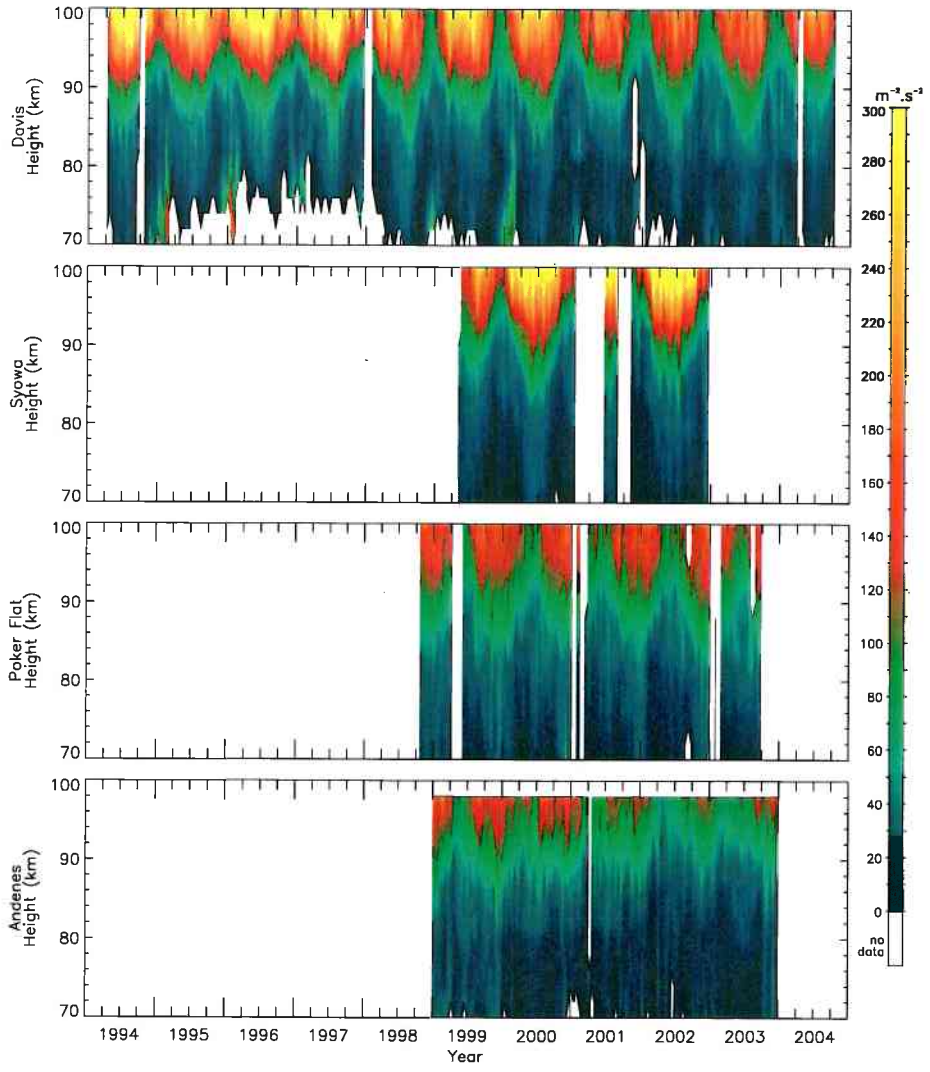

Figure 2.7: As for Figure 2.6, but for the meridional variances in the period range 20-120 minutes.

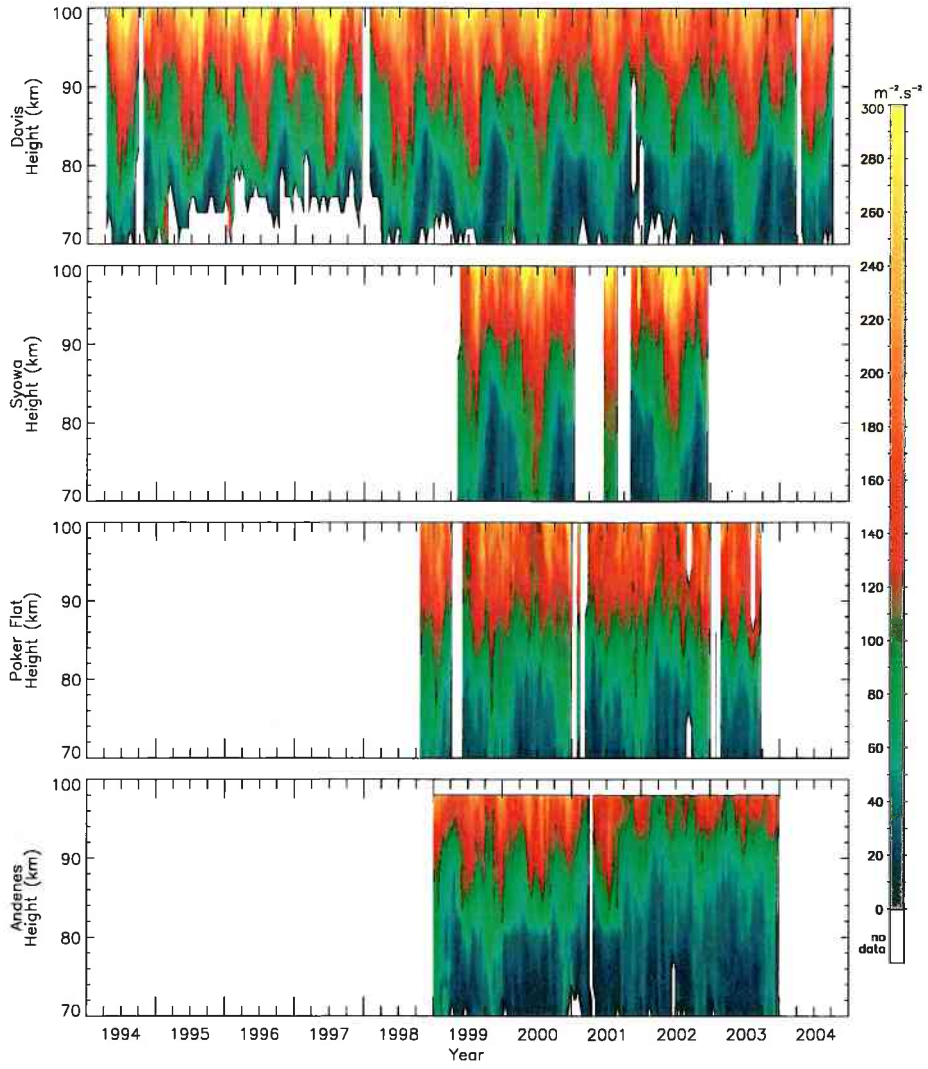

Figure 2.8: As for Figure 2.6, but for the zonal variances in the period range 120-480 minutes.

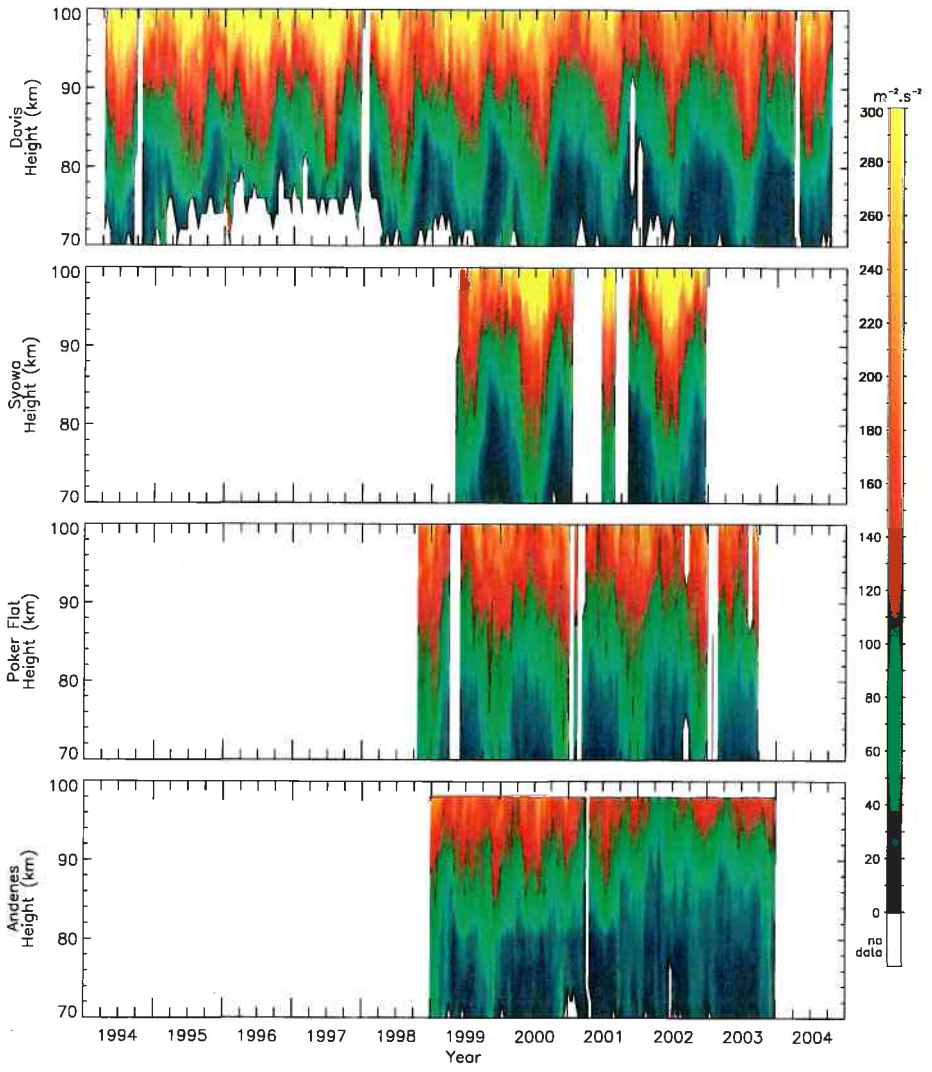

Figure 2.9: As for Figure 2.6, but for the meridional variances in the period range 120-480 minutes.

Chapter 3

Mean wind climatology

3.1 Introduction

Horizontal wind fields obtained from MF radar observations at Davis, Syowa and Rothera in the Antarctic and Poker Flat and Andenes in the Arctic were shown previously in Figures 2.2 and 2.3. The multiple years of data available from the MF radars located at Davis and Syowa, Poker Flat and Andenes allow mean wind climatologies to be produced at these locations. Only four months of data were made available from Rothera (specifically for the purpose of investigating the 2002 southern hemisphere major stratospheric warming) and so Rothera is not included in the climatological investigations presented here.

Mean zonal and meridional wind climatologies are estimated by averaging together all available years of data. The timing and magnitude of various climatological features are investigated. Inter-hemispheric comparisons are made and discussed in terms of their implications for the MLT region.

A comparison of mean winds in the northern and southern polar MLT was previously published as part of this PhD research in *Dowdy et al.* [2001]. Data were presented only from Davis and Poker Flat from 1999 until mid-2000 (due to the availability of data at that time). The published results are consistent with the results presented in this chapter, with only small differences as is expected from averaging

over different time intervals.

3.2 Zonal wind climatologies

Figure 3.1 shows climatologies of the zonal winds at Davis, Syowa, Poker Flat and Andenes. Data are used only when at least 20 hours of data is available on a particular day to minimise the influence of tides due to consistent hour gaps. The climatologies are produced by averaging daily wind data over all available years. Data are shown only if there were 2 or more years available to produce the average for a particular height and day. A 15-day and 4-km running mean is applied.

Various features are apparent in the zonal wind climatology shown in Figure 3.1. It can be seen that the mesospheric zonal winds are generally eastward in winter and westward in summer at each of the four locations.

The spring transition from the eastward winds of winter to the westward winds of summer shows some hemispheric differences. The boundary between the eastward and westward winds has a downward phase progression at the northern hemisphere locations, descending in height over a period of about a month. This is not observed at the two southern hemisphere locations where the change occurs more simultaneously throughout the MLT region.

The change in the zonal winds going from summer to winter also shows some interesting features. The zonal winds at Syowa and Poker Flat become westward in the lower thermosphere for a brief period near the end of summer (early March at Syowa and late September at Poker Flat). This is not a feature of the climatologies at Davis or Andenes.

3.2.1 Summer zonal wind climatology

The zonal winds are generally negative during summer in the mesosphere at all four locations, with positive winds at higher altitudes. The boundary between the westward and eastward summer winds descends in height through the lower thermosphere during

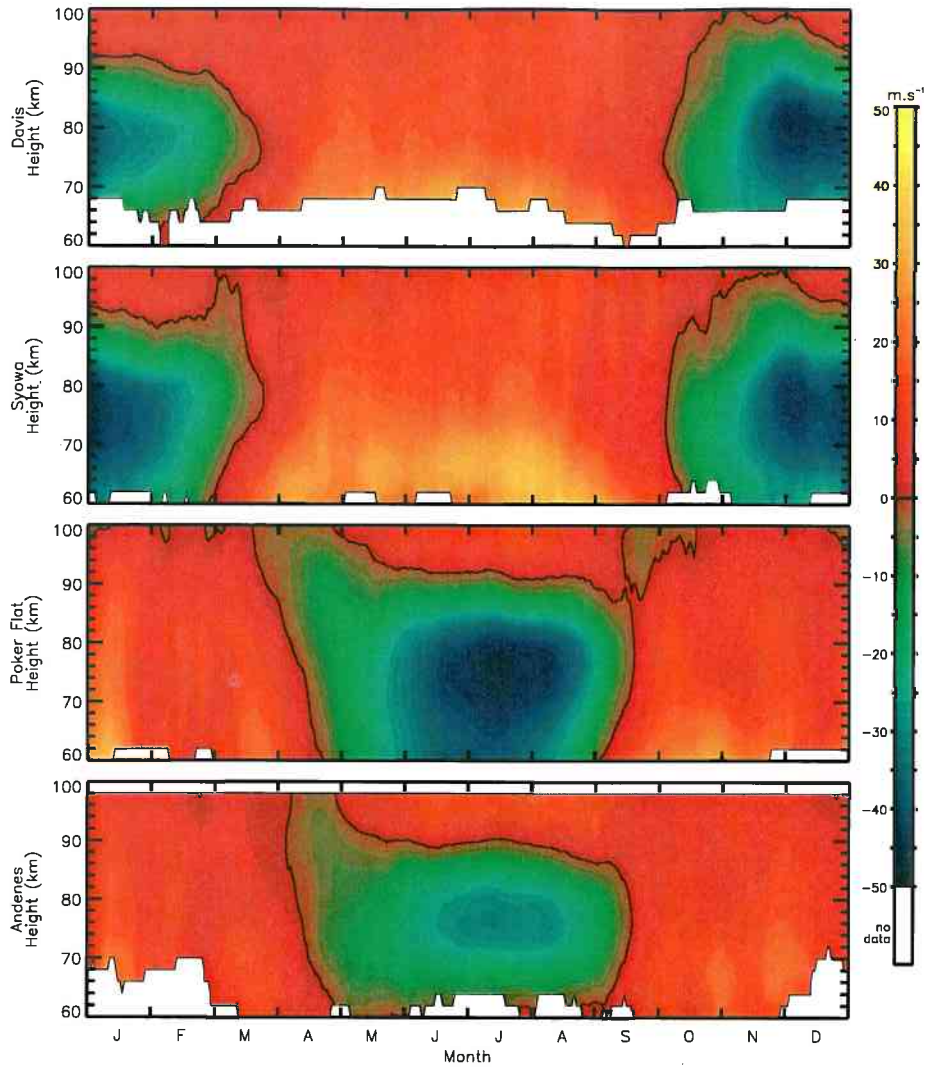

Figure 3.1: Zonal wind climatologies for Davis, Syowa, Poker Flat and Andenes. A 15-day and 4-km running mean is applied.

summer. The descent of this boundary begins around the start of December at both Antarctic locations, which is about 20 days prior to the southern summer solstice (December 21). The descent of this boundary begins around the start of May at both Arctic locations. This is about 50 days prior to the northern summer solstice (June 21), giving a hemispheric difference of about 30 days with respect to the summer solstices.

In the mesosphere during summer, the westward winds peak at a height about 10

Location	Date	Days from summer solstices	Height (km)	Magnitude (ms^{-1})
Davis	December 8	-13	80	-45
Syowa	January 1	11	78	-45
Poker Flat	July 16	25	76	-48
Andenes	July 14	23	76	-30

Table 3.1: The timing, height and magnitude of the peak westward zonal winds during summer at Davis, Syowa, Poker Flat and Andenes (as determined from the climatologies shown in Figure 3.1).

km beneath the mesopause at all four locations. The date, height and magnitude of the peak westward wind at each location is shown in Table 3.1 as determined from the climatologies shown in Figure 3.1. The timing of the peak is also shown with positive (negative) values for days after (before) the summer solstice of each hemisphere.

Figure 3.1 shows that the westward winds at Syowa appears to have a double peak during summer. The first peak occurs before the summer solstice at about the same time as the peak at Davis, while the second peak occurs shortly after the summer solstice. The second peak is larger than the first and has therefore been used for the information presented in Table 3.1.

Table 3.1 shows that the peak westward winds occur on average about 25 days earlier with respect to the summer solstice at the Antarctic locations than at the Arctic locations. The peaks occur slightly higher (by about 3 km on average) at the Antarctic locations than at the Arctic locations.

The magnitudes of the westward wind peaks at Davis, Syowa and Poker Flat are reasonably similar to each other, but about 50% larger than at Andenes where the winds tend to be weaker in general. The peak magnitude at Poker Flat is $\sim$3 ms^{-1} stronger than at Davis and Syowa.

3.2.1.1 Time profiles of the summer zonal wind peak

Figure 3.2 details the time evolution of the westward zonal wind peak during summer at each location. The data shown are taken from the climatologies of Figure 3.1 at the

Location	Start of jet (date)	Start of jet (days from solstice)	End of jet (date)	End of jet (days from solstice)
Davis	October 17	-75	March 22	91
Syowa	October 15	-77	March 26	95
Poker Flat	April 13	-69	September 20	91
Andenes	April 14	-68	September 19	90

Table 3.2: Starting and ending dates of the westward zonal winds during summer at Davis, Syowa, Poker Flat and Andenes (as determined from the data shown in Figure 3.1 for the heights shown in Table 3.1).

height of the peak westward winds at each location as listed in Table 3.1. The dotted lines indicate the standard error in the mean, $\Delta\overline{u}$, given by:

$$\Delta\overline{u} = \frac{\sigma}{\sqrt{n}} \tag{3.1}$$

where: σ is the standard deviation of the sample,

and n is the sample size (the number of years of available data).

It is apparent from Figure 3.2 that the peak westward winds occur significantly earlier ($\sim$25 days) at the southern hemisphere locations than at the northern hemisphere locations relative to the summer solstices, as mentioned previously. Such a large hemispheric difference does not occur for the starting or ending dates of the period of westward winds during summer, as is detailed in Table 3.2.

Prior to the westward wind maxima, the acceleration of the zonal winds is larger at the Antarctic locations (0.60 $\mathrm{ms^{-1}day^{-1}}$) than at the Arctic locations (0.42 $\mathrm{ms^{-1}day^{-1}}$). After the westward wind maxima, the deceleration is larger at the Arctic locations (0.59 $\mathrm{ms^{-1}day^{-1}}$) than at the Antarctic locations (0.48 $\mathrm{ms^{-1}day^{-1}}$).

The jet starts about a week earlier and ends about 3 days later at the Antarctic locations than it does at the Arctic locations (on average with respect to the summer solstices). This is much smaller than the $\sim$25 day hemispheric difference observed for the timing of the peak westward winds. This means that the period of winter eastward

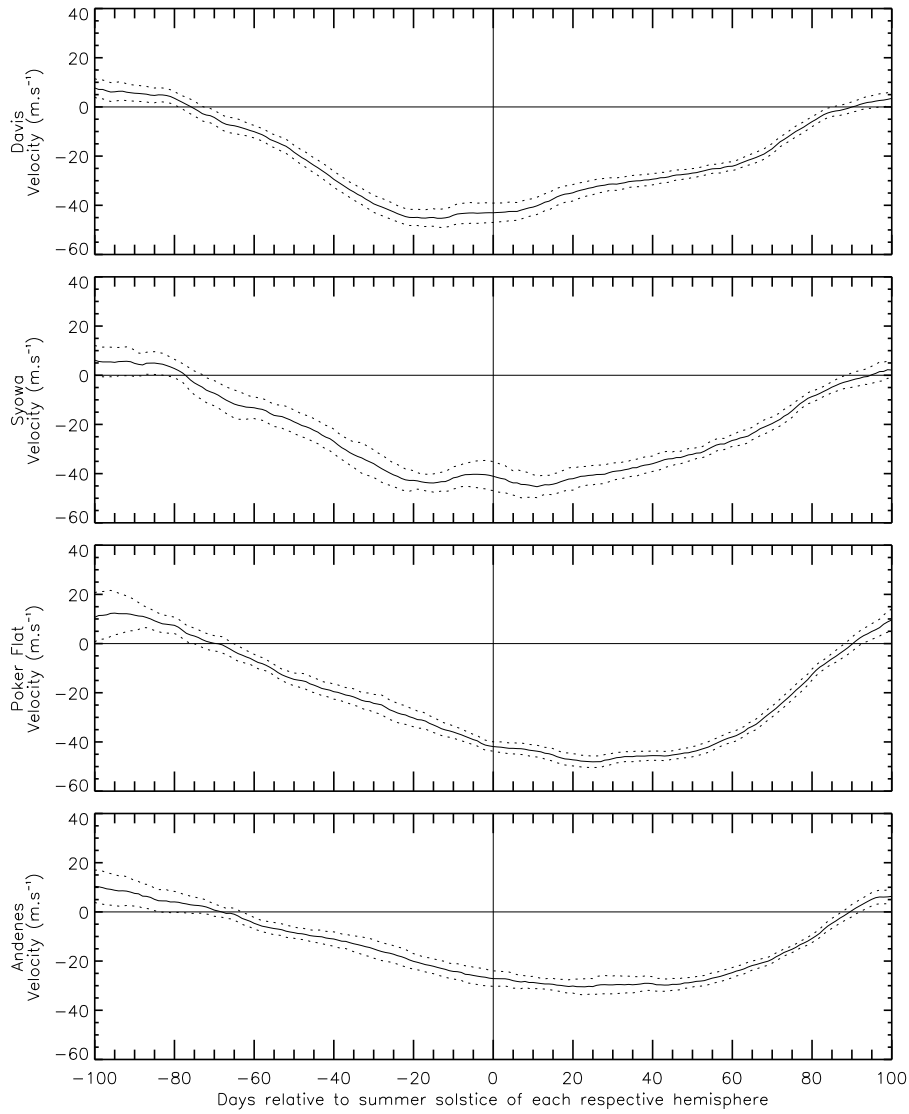

Figure 3.2: Time series of the zonal wind climatologies shown in Figure 3.1 at heights corresponding to the peak summer westward winds as listed in 3.1. The dotted lines indicate the standard error in the mean.

winds is about 10 days shorter in the Antarctic than in the Arctic.

3.2.1.2 Height profiles of the summer zonal wind peak

Figure 3.3 shows height profiles of the summer westward wind peaks. As mentioned previously, the peaks occur only slightly higher (by about 3 km) at the southern hemisphere locations than at the northern hemisphere locations, and the magnitude

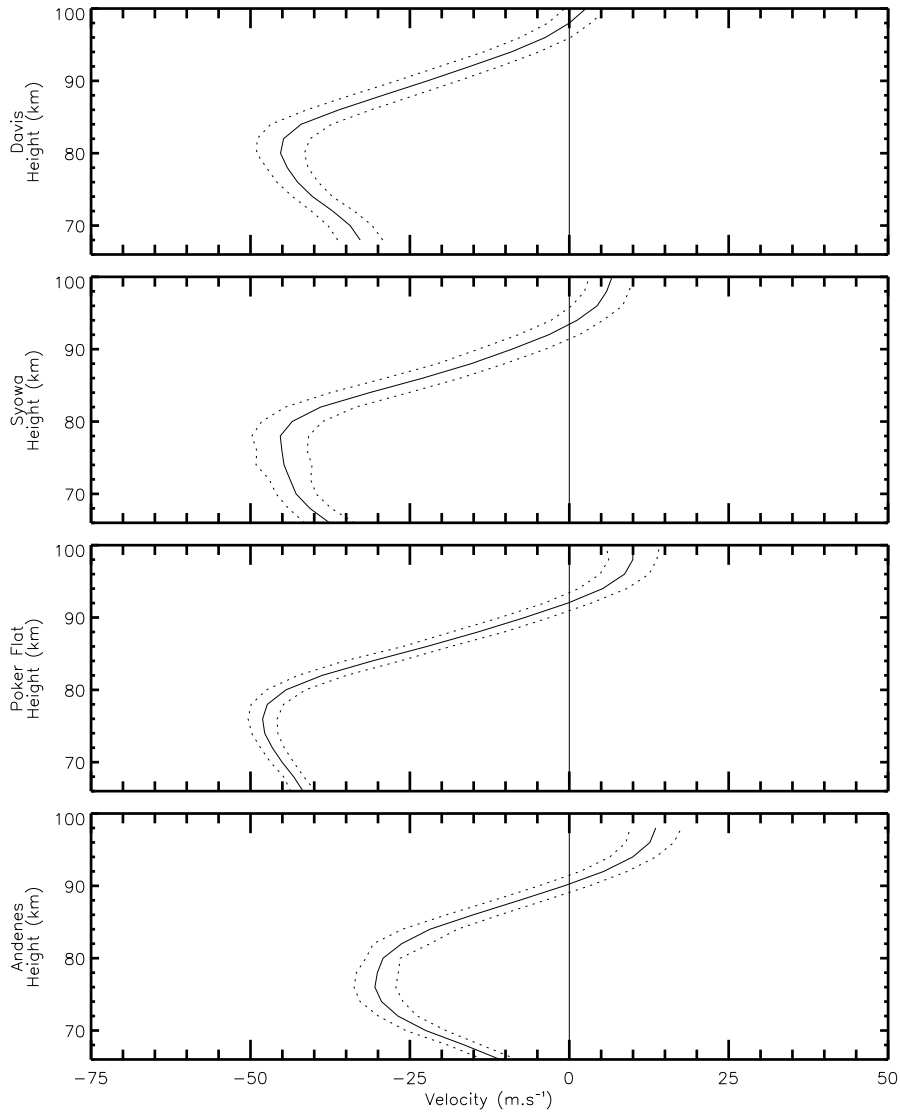

Figure 3.3: Height profiles detailing the peak westward zonal winds during summer at Davis, Syowa, Poker Flat and Andenes (using the data shown in Figure 3.1 for the dates shown in Table 3.1). The dotted lines indicate the standard error in the mean.

of the peaks at Davis, Syowa and Poker Flat are all about 50% larger than at Andenes.

3.2.2 Winter zonal wind climatology

In contrast to what was observed during summer, a large peak does not occur in the magnitude of the zonal winds during winter (see Figure 3.1). The zonal winds tend to be larger at the lower heights during winter, with significantly larger magnitudes

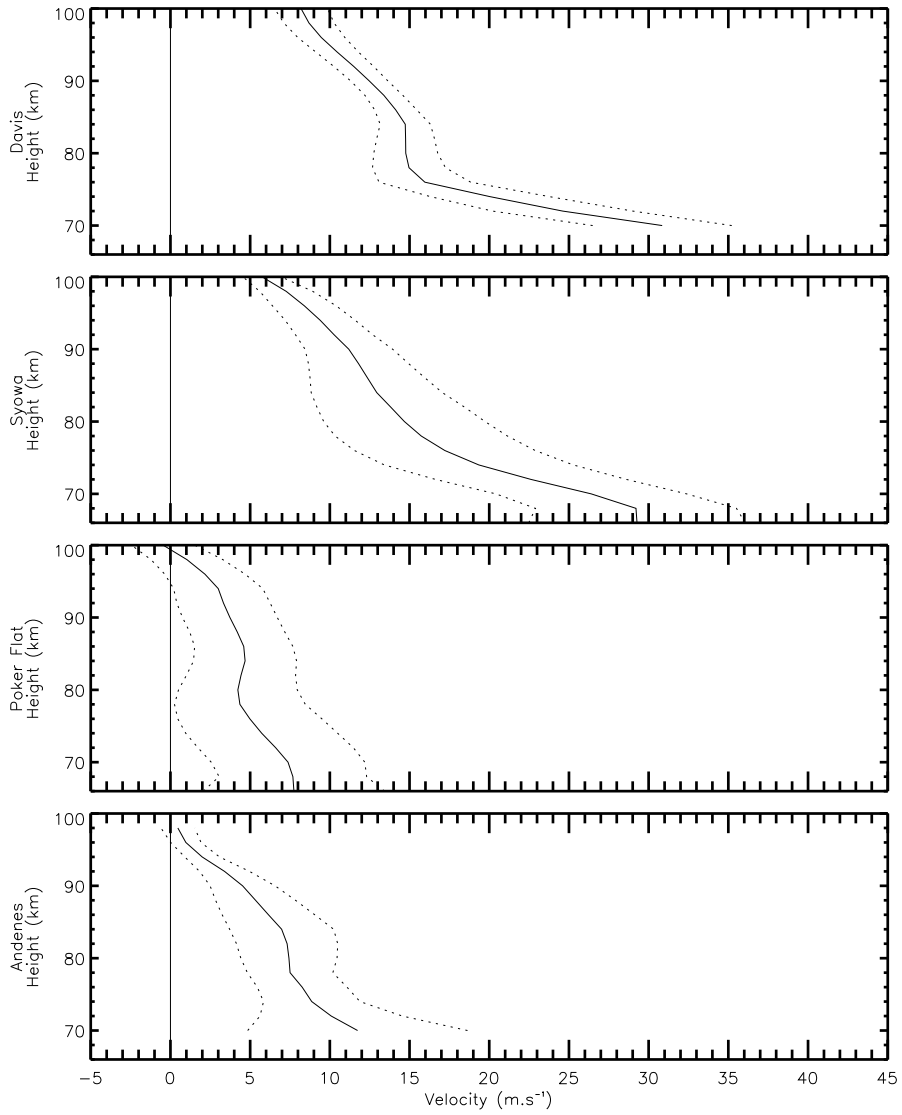

Figure 3.4: Height profiles of the zonal wind climatologies (shown in Figure 3.1) at Davis, Syowa, Poker Flat and Andenes on the winter solstices. The dotted lines indicate the standard error in the mean.

at the southern hemisphere locations than at the northern hemisphere locations. This hemispheric difference is detailed in Figure 3.4 which shows height profiles of the zonal wind climatologies (shown in Figure 3.1) on the winter solstice in each hemisphere. The dotted lines indicate the standard error in the mean.

It is apparent from Figure 3.4 that the eastward winds are significantly stronger

Location	Date	Days from summer solstice	Height (km)	Magnitude (ms^{-1})
Davis	January 1	11	88	10
Syowa	December 27	6	88	12
Poker Flat	July 1	10	88	-16
Andenes	July 5	14	86	-8

Table 3.3: Date, height and magnitude of the peak equatorward meridional winds during summer at Davis, Syowa, Poker Flat and Andenes (as determined from the climatologies shown in Figure 3.5).

throughout the MLT at the southern hemisphere locations than at the northern hemisphere locations (similar to CIRA-86, see Figure 1.3). This difference is about 20 ms^{-1} at ∼70 km, and about 8 ms^{-1} at ∼90 km. The zonal wind shear is larger throughout the MLT at the Antarctic locations than at the Arctic locations, with the largest hemispheric difference in the zonal wind speed occurring at the lower heights.

3.3 Meridional wind climatologies

Figure 3.5 is similar to Figure 3.1, but for the meridional winds. Some seasonal variations are evident in the meridional wind climatologies (Figure 3.5), although they are generally not as large in magnitude or as well defined in direction as was the case for the zonal winds. The meridional winds are generally weaker in strength and more variable in direction than the zonal winds.

3.3.1 Summer meridional wind climatology

At all four locations during summer, the meridional wind climatologies (Figure 3.5) show an equatorward peak, northward (positive) in the Antarctic, and southwards (negative) in the Arctic. The date, height and magnitude of the peak in the equatorward jet at each location are shown in Table 3.3 (as determined from the climatologies shown in Figure 3.5).

From Table 3.3 it is apparent that the height of the equatorward wind peak is

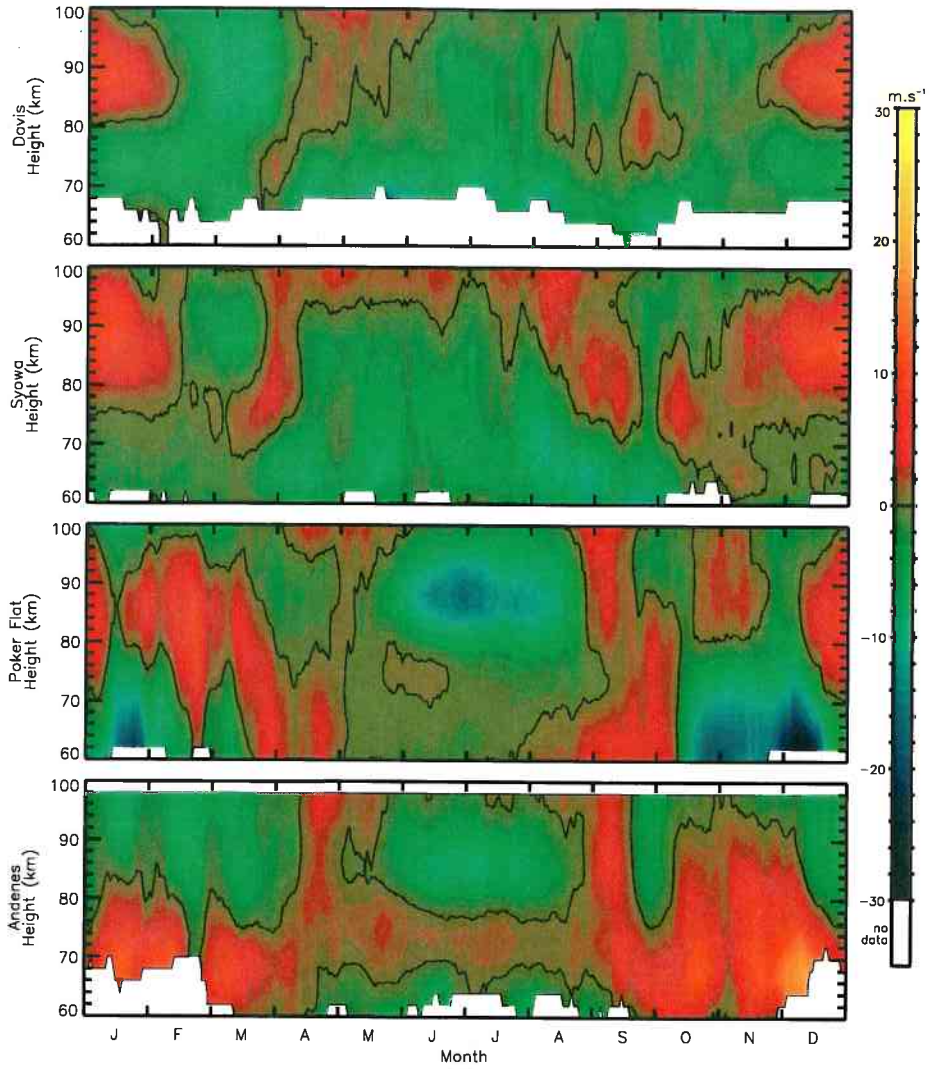

Figure 3.5: As for Figure 3.1, but for the meridional winds.

similar at all four locations (86-88 km). Of the four locations the peak magnitude is largest at Poker Flat and smallest at Andenes, as was also the case for the westward zonal wind peak during summer. The meridional wind peak occurs only about ~4 days earlier on average at the Antarctic locations than at the Arctic locations (with respect to the summer solstices), much less than the ~25 day hemispheric difference observed for the timing of the zonal wind peak during summer.

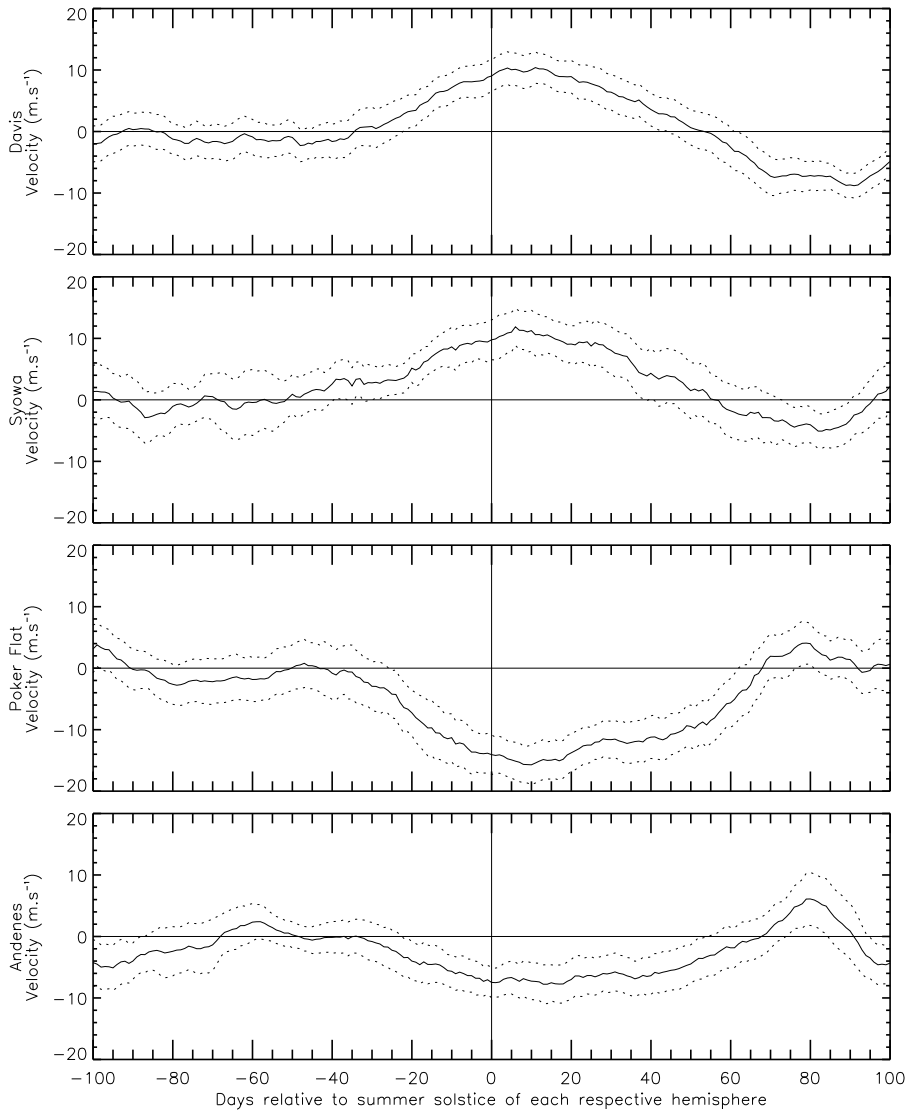

Figure 3.6: Meridional wind time series (for the climatologies shown in Figure 3.5) at heights corresponding to the peak summer westward winds (as listed in Table 3.3). The dotted lines indicate the standard error in the mean.

3.3.1.1 Time series of the summer meridional wind peak

Time series of the meridional winds are shown in Figure 3.6, detailing the equatorward peak that occurs during summer. The data shown are from Figure 3.5 at the height of the peak equatorward winds at each location (as listed in Table 3.3). The standard error in the mean is indicated by the dotted lines.

The starting and ending dates of the peak equatorward meridional winds during

Location	Start of jet (date)	Start of jet (days from summer solstice)	End of jet (date)	End of jet (days from summer solstice)
Davis	November 17	-34	February 13	54
Syowa	October 31	-51	February 15	56
Poker Flat	May 9	-43	August 28	68
Andenes	May 19	-33	August 28	68

Table 3.4: Starting and ending dates of the peak equatorward meridional winds during summer at Davis, Syowa, Poker Flat and Andenes (as determined from the data shown in Figure 3.5).

summer are shown in Table 3.4 (as determined from the data shown in Figure 3.5). A large hemispheric timing difference occurs for the time that the equatorward jet ends. The equatorward jet persists for ∼13 days longer on average after the summer solstice at the Arctic locations than at the Antarctic locations. Such a large hemispheric timing difference does not occur for the start or the peak of the equatorward jet, with the jet starting only ∼5 days later on average at the Arctic locations than at the Antarctic locations.

3.3.1.2 Height profiles of the summer meridional wind peak

Figure 3.7 shows height profiles of the equatorward wind peaks (using the climatologies shown in Figure 3.5 for the dates shown in Table 3.3). The dotted lines indicate the standard error in the mean. The peak equatorward winds occur at about the same height (86-88 km) at all four locations, which is about 10 km higher than the zonal wind peak which occurs at about 76-80 km.

The height of the meridional equatorward summer jet is similar to the height of maximum zonal wind shear (also see *Manson et al.* [1991]). Figure 3.8 shows the zonal wind shear determined by taking the height differential of the zonal wind climatology (Figure 3.1). The zonal wind shear and the equatorward jet both maximise during summer around 88 km at all four locations.

3.3.2 Winter meridional wind climatology

The meridional winds during winter at Poker Flat and Andenes are often opposite in sign to each other (see Figure 3.5). This is consistent with quasi-stationary zonal wave-1 planetary wave activity since the two Arctic locations are almost 180° different in longitude to each other[1].

The quasi-stationary planetary wave signatures in the Arctic MLT appears to have a vertical wavelength greater than ∼40 km. At heights around 70 km the meridional winds during winter are generally southward at Poker Flat and northward at Andenes, with the converse often being the case at heights around 90 km (Figure 3.5).

The meridional winds at the two Antarctic locations are generally not as strong as at the Arctic locations. Significant quasi-stationary planetary wave signatures during winter are not seen in the meridional winds at the Antarctic locations, although the two locations are only separated in longitude by 38°.

3.4 Implications of hemispheric comparisons

The differences observed between the wind climatologies of the southern and northern hemispheres suggest that hemispheric differences may also exist for the processes which drive the mean winds in the MLT, such as gravity wave forcing. It has been suggested that the meridional wind could be used as a proxy for gravity wave driving in computing the strength of the mean vertical motions [*Dowdy et al.*, 2001]. This should be a valid assumption in the summer MLT since forced planetary waves are excluded by the westward winds at lower heights (see Equation 1.32), and transient waves such as the 2-day wave appear to induce equatorward winds of only about 1 ms^{-1} [*Lieberman*, 1999].

Temperatures in the summer polar MLT are a balance between the radiative spring, and the adiabatic cooling resulting from the rising motions (upwelling) over the pole due to gravity wave momentum deposition. This is investigated in the following two

[1]The difference in longitude between Poker Flat and Andenes is 163°.

sections. The longer persistence of the summer equatorward jet in the Arctic than in the Antarctic suggests that hemispheric differences in adiabatic cooling might exist. This in turn implies hemispheric differences in the occurrence of temperature dependent phenomena such as PMSEs, PMCs and NLCs might also exist. This theory is investigated further in the following 2 sections.

3.4.1 PMC observations

PMC data were made available from the Summer Mesospheric Explorer (SME) satellite at 70°N and 70°S (see *Olivero & Thomas* [1986] for details). Figure 3.9 shows the frequency of PMC observation at these latitudes on average over the years 1982-1986. Data are plotted with respect to the date of the summer solstice of each hemisphere. The mean starting and ending dates of the equatorward meridional jet (from Table 3.4) are also shown dotted in red for Poker Flat and Andenes, and in blue for Davis and Syowa.

Figure 3.9 shows that PMC observations begin at about the same time (with respect to the summer solstices) in each hemisphere. The frequency of observations increase at about the same rate in both hemispheres leading up to the summer solstice (during December in the Antarctic, and June in the Arctic).

The observation frequencies after the summer solstices become significantly larger in the Arctic than in the Antarctic. The peak frequency of observation is about 15% higher in the Arctic (∼58%) than in the Antarctic (∼43%). It might therefore be expected that the peak magnitude of the equatorward jet would be larger in the Arctic than in the Antarctic (using the meridional winds as a proxy for gravity wave driving and consequent adiabatic cooling). This however is not the case, with the average magnitude of the equatorward jet being -12 ms^{-1} for the Antarctic locations and 11 ms^{-1} for the Arctic locations. A simple relationship might not be expected if the process is non-linear, an example being if outward flow greater than some value triggers PMC formation.

The peak PMC observation frequency occurs about 17 days after the summer

solstice in both hemispheres. The fact that a large hemispheric timing difference does not occur is consistent with the timing of the peak equatorward jet, which was found to occur at about the same time ($\sim$10 $\pm$ 4 days after the summer solstice) at all four locations.

The frequency of PMC observations decreases during February in the Antarctic and August in the Arctic, with PMC observations remaining about 15% more frequent in the Arctic than in the Antarctic. During this time, the frequency of observation in the Arctic is similar to the frequency of observation in the Antarctic about 2 weeks earlier.

The longer persistence (after the summer solstice) of PMCs in the northern hemisphere is, in this way, similar to the longer persistence of the summer equatorward meridional jet in the northern hemisphere (as indicated by the dotted lines in Figure 3.9). This is reasonably consistent with the theory that the meridional winds can be used as a proxy for the adiabatic cooling associated with gravity wave drag in this region.

3.4.2 PMSE observations

A VHF radar was recently installed at Davis, with the 2003/2004 summer being the first summer of operations [*Morris et al.*, 2004]. PMSEs were observed by the VHF radar during this summer as detailed in Figure 3.10.

Figure 3.11 shows the summer equatorward jet at Davis (from Figure 3.5), with the dotted lines indicating the starting and ending dates of PMSE observations made at Davis during the 2003/2004 southern summer.

The starting and ending dates of the PMSE observations are relatively consistent with the starting and ending dates of the meridional equatorward wind flow at Davis. The equatorward jet starts $\sim$2 days earlier and ends $\sim$8 days earlier than the period of PMSE observations. This is reasonably consistent with the theory that the mean meridional winds can be used as a proxy for the adiabatic cooling associated with gravity wave drag in this region.

3.5 Discussion and summary

Mean wind climatologies at Davis, Syowa, Poker Flat and Andenes were investigated in this Chapter. Differences were found between the four locations in the strength, timing and height of the various features present in the wind climatologies. The observed differences were often hemispheric in nature.

The zonal winds are generally eastward during winter and westward during summer at all four locations. The winter-summer transition of the zonal winds descends in height over a period of about a month at the northern hemisphere locations, but is more rapid at the southern hemisphere locations.

The westward zonal winds during summer maximise at heights between 76-80 km at all four locations. This occurs on average about 1 day prior to the summer solstice at the southern hemisphere locations, and about 25 days later in the Arctic. This large timing difference was found to be due to a greater acceleration of the mean winds during early summer at the southern hemisphere locations (0.60 ms^{-2}) than at the northern hemisphere locations (0.42 ms^{-2}). The deceleration of the zonal winds following the summer peak was found to be larger in the Arctic (0.59 ms^{-2}) than in the Antarctic (0.48 ms^{-2}), with the change in the zonal winds to the eastward direction occurring at about the same time (92 $\pm$ 3 days) relative to the summer solstice at all four locations.

During winter, the zonal winds in the MLT are significantly stronger in the Antarctic than in the Arctic (a difference of $\sim$8 ms^{-1} at heights around 90 km, and $\sim$20 ms^{-1} at a heights around 70 km). Weaker zonal winds during winter in the Arctic than in the Antarctic can be related to a hemispheric difference in planetary wave activity and sudden stratospheric warmings (as is investigated in Chapter 6). In addition to this, the topography of the Antarctic continent itself (a pole centred dome) also contributes to a more stable zonal circulation at all levels of the atmosphere compared to that of the north where ocean currents and continental topography create considerable variability.

The meridional wind climatologies during winter show differences between the two northern hemisphere locations consistent with the presence of quasi-stationary wave-1 planetary wave activity. The meridional winds are generally southward at Poker Flat and northward at Andenes at about 70 km during winter, with the converse being the case around 90 km, suggesting a vertical wavelength greater than about ∼40 km.

Quasi-stationary planetary wave signatures do not appear to be a feature of the meridional wind climatologies at the southern hemisphere locations, although this is difficult to determine since Davis and Syowa are relatively close in longitude to each other. The meridional winds at the southern hemisphere locations are generally weaker than at the northern hemisphere locations throughout the winter MLT.

A peak in the meridional winds is observed during summer in an equatorward direction at all locations (southward in the Arctic, and northward in the Antarctic). The peak equatorward jet occurs only about ∼4 days earlier on average at the Antarctic locations than at the Arctic locations (with respect to the summer solstice in each hemisphere).

The equatorward jet was found to persist for about 2 weeks longer after the summer solstice in the Arctic than in the Antarctic. If the meridional winds can be used as a proxy for gravity wave driving and consequent adiabatic cooling [*Dowdy et al.*, 2001], then the longer persistence of the equatorward jet in the Arctic would suggest that cold MLT temperatures might persist for longer in the Arctic than in the Antarctic.

This hypothesis was found to be reasonably consistent with PMC observations from the SME satellite. Towards the end of summer PMC observations in the Arctic were found to be similar in frequency to observations about 2 weeks earlier (with respect to the summer solstice) in the Antarctic.

Further support for this hypothesis is that the starting and ending dates of the PMC observations are similar to the starting and ending dates of the equatorward jet. This is also the case for PMSE observations made with the VHF radar at Davis.

The peak magnitude of the equatorward jet varies somewhat between the four locations, ranging from a minimum of 10 ms^{-1} at Andenes to a maximum of 17 ms^{-1}

at Poker Flat. Although this is only a small sample in longitude, this range of values is reasonably consistent with the model results of *Fritts & Luo* [1995] who report a mean meridional jet of approximately 10-15 ms^{-1}, corresponding to a mean vertical motion of approximately 0.05 ms^{-1} due to gravity wave forcing.

Gardner et al. [2001] suggest that hemispheric differences exist in the altitude of PMC occurrence from lidar temperature measurements made at the north and south poles. The altitudes of PMCs over the South Pole are reported to be consistently 2-3 km higher than those observed over the North Pole. *Chu et al.* [2003] report that PMCs occur about 1 km higher in the southern hemisphere than at similar latitudes in the northern hemisphere. This implies that a small (not resolvable by the MF radars) hemispheric difference in the height of the summer equatorward jet may exist. The MF radars used in this study have an effective height resolution of 4 km, and measured the peak of the equatorward jet to be between 86-88 km at all four locations.

There is some debate as to whether or not significant differences do indeed occur between the temperature structures of the Arctic and Antarctic MLT. Satellite measurements suggest that the southern hemisphere mesopause is a few degrees warmer than in the north [*Huaman & Balsley*, 1999]. Recent rocket studies found summer mesopause temperatures in the Arctic and Antarctic to be significantly different towards the end of summer (February in the southern hemisphere, and August in the northern hemisphere), but quite similar earlier on (January in the southern hemisphere, and July in the northern hemisphere) [*Lübken et al.*, 1999; *Lübken et al.*, 2004].

Significant hemispheric differences have also been reported in the occurrence of phenomena that rely on cold mesopause temperatures during the polar summers. A lack of PMSE in the southern hemisphere was suggested by *Balsley et al.* [1995] from VHF radar observations in the high latitudes of the southern hemisphere. Observations from a VHF radar recently installed at Davis, Antarctica have shown strong PMSE activity [*Morris et al.*, 2004]. Hemispheric differences have been observed in the occurrence of PMC, with the northern hemisphere clouds generally being brighter and

occurring over a larger range (by about 5° latitude) than in the southern hemisphere [*Olivero & Thomas*, 1986; *Thomas & Olivero*, 1989].

It has been seen in this chapter that phenomena such as the peaks in both the zonal and meridional winds during summer occur earlier (closer to the summer solstice) in the southern hemisphere than in the northern hemisphere. The greater symmetry around the solstice indicates that radiative effects may play a larger role in controlling the state of the southern polar MLT than in the northern hemisphere, where dynamical effects could be more important.

Given the role that gravity wave drag plays in closing the zonal jet and driving the meridional circulation, the hemispheric differences in the zonal and meridional winds suggest that wave driving (and consequent adiabatic cooling) may be different between the two hemispheres. This is investigated further in the following chapter.

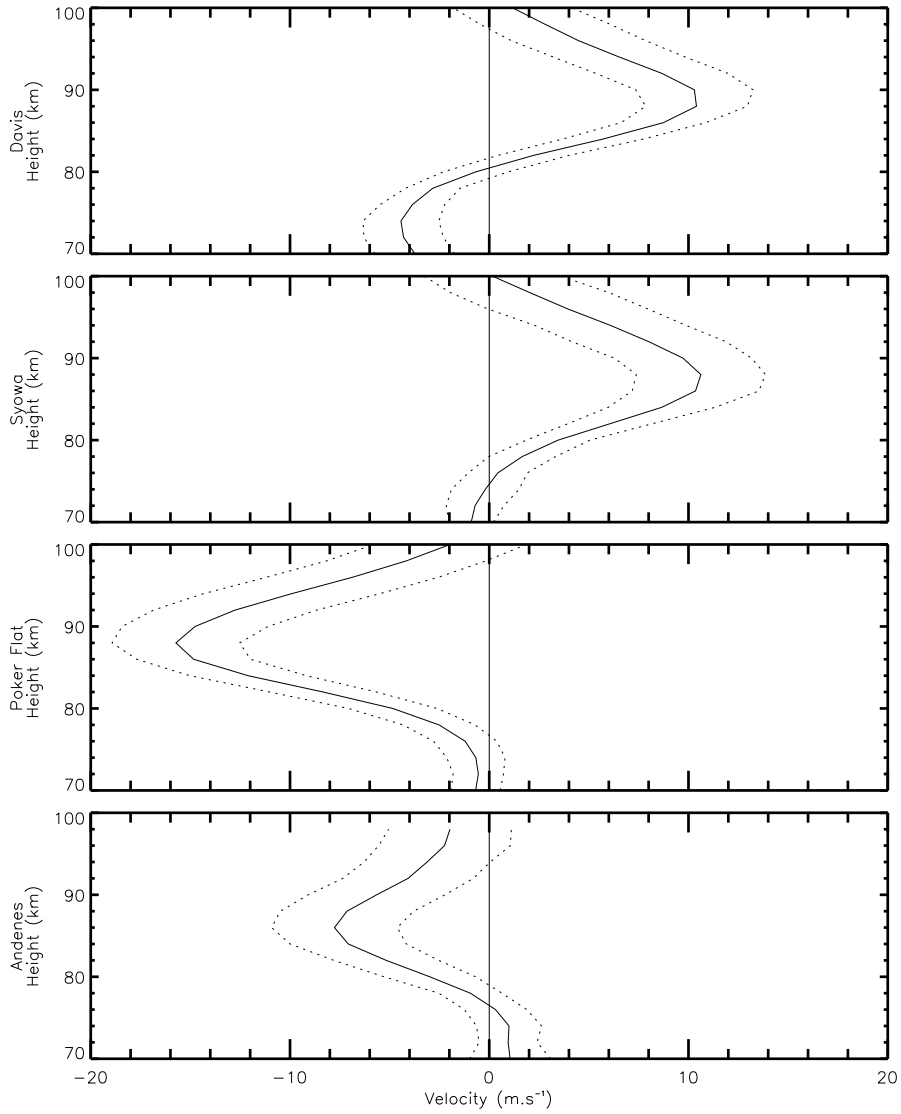

Figure 3.7: Height profiles detailing the equatorward peak meridional winds during summer at Davis, Syowa, Poker Flat and Andenes (using data from Figure 3.5 for the dates corresponding to the peak summer westward winds as listed in Table 3.3). The standard error in the mean is indicated by the dotted lines.

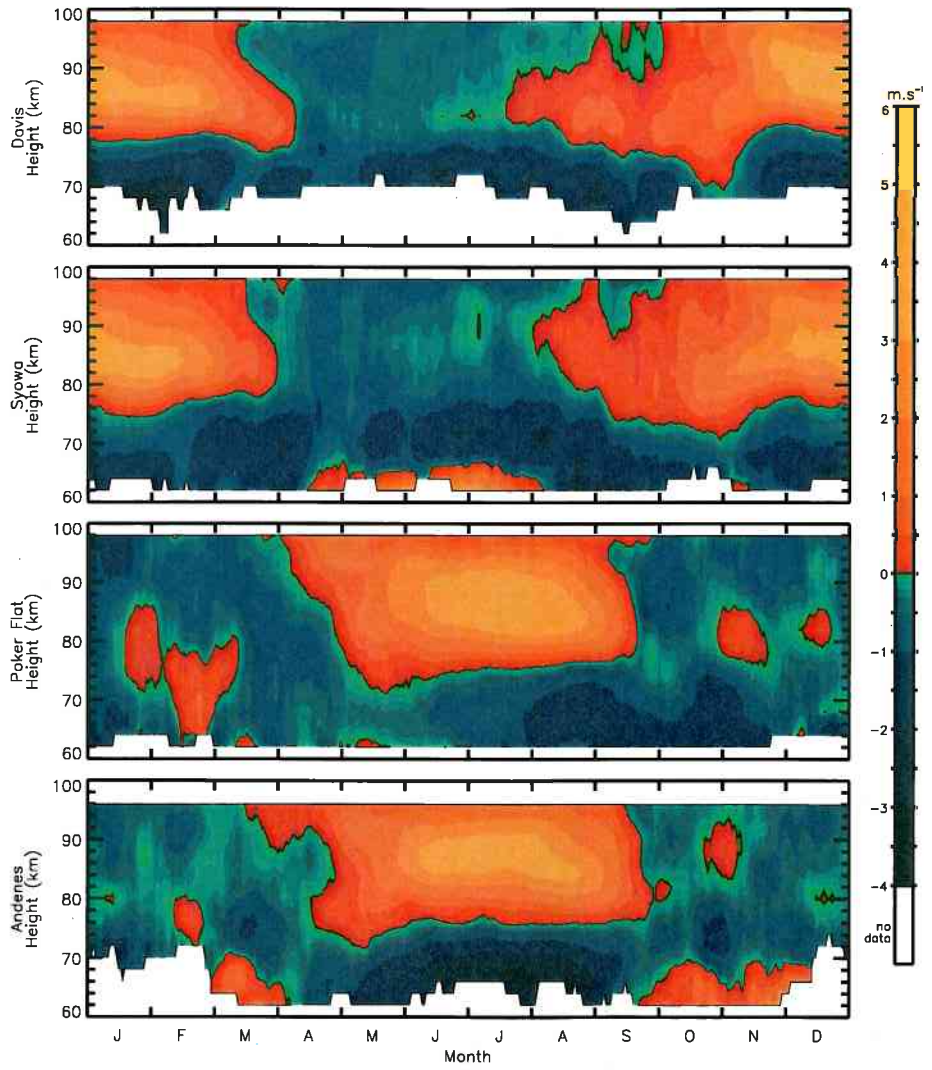

Figure 3.8: The zonal wind shear at Davis, Syowa, Poker Flat and Andenes, produced from the height differentials of the zonal wind climatologies shown in Figure 3.1.

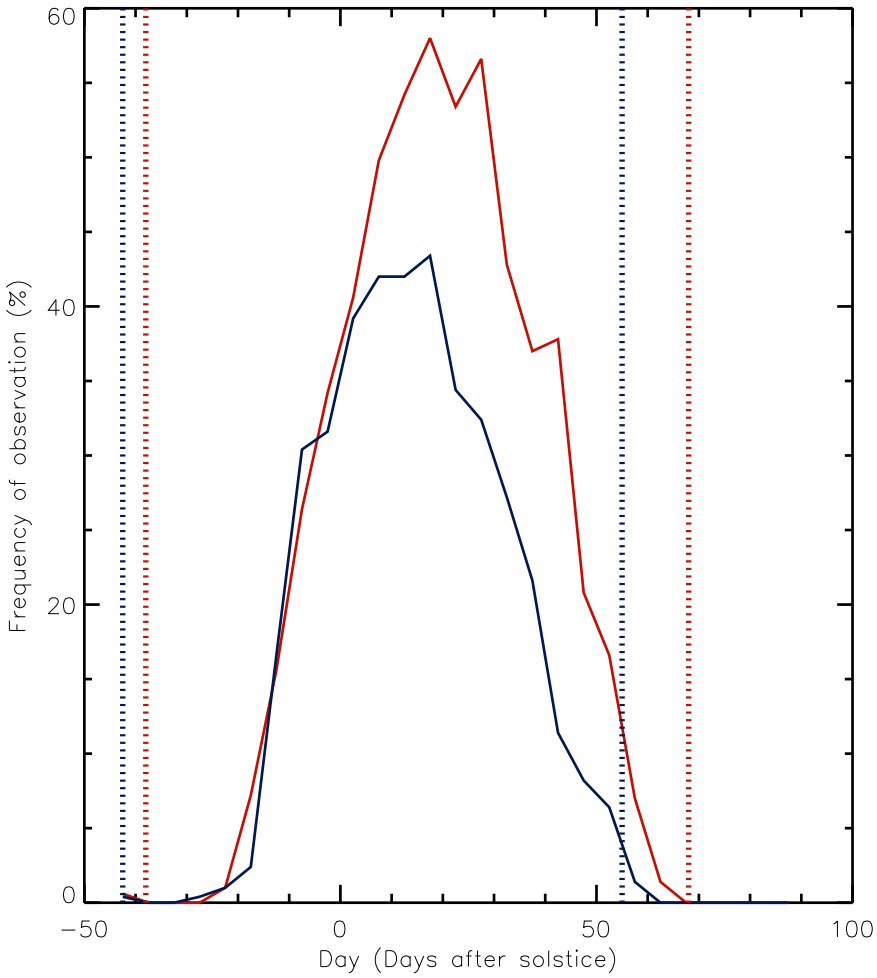

Figure 3.9: PMC observation frequency from the Summer Mesospheric Explorer satellite. Data are shown from 70°N in red, and from 70°S in blue. The mean starting and ending dates (relative to the summer solstice) of the equatorward meridional jet are shown dotted in red for Poker Flat and Andenes, and in blue for Davis and Syowa (for the heights shown in Table 3.4).

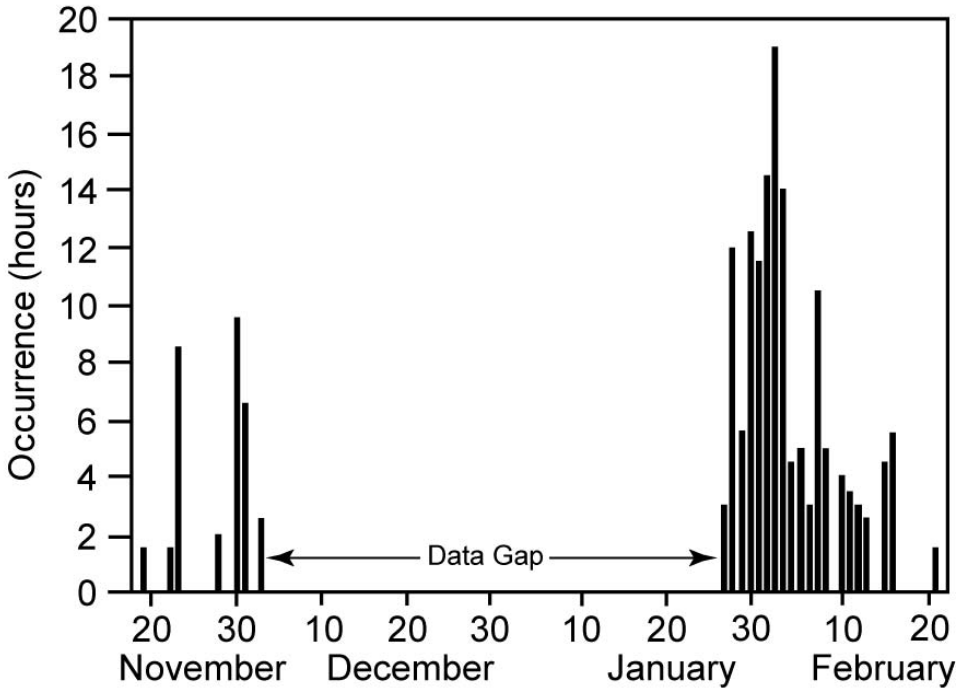

Figure 3.10: Seasonal occurrence histogram of PMSE observed at Davis from 19 November until 3 December 2003 and from 27 January until 21 February 2004 (from *Morris et al.*, 2004).

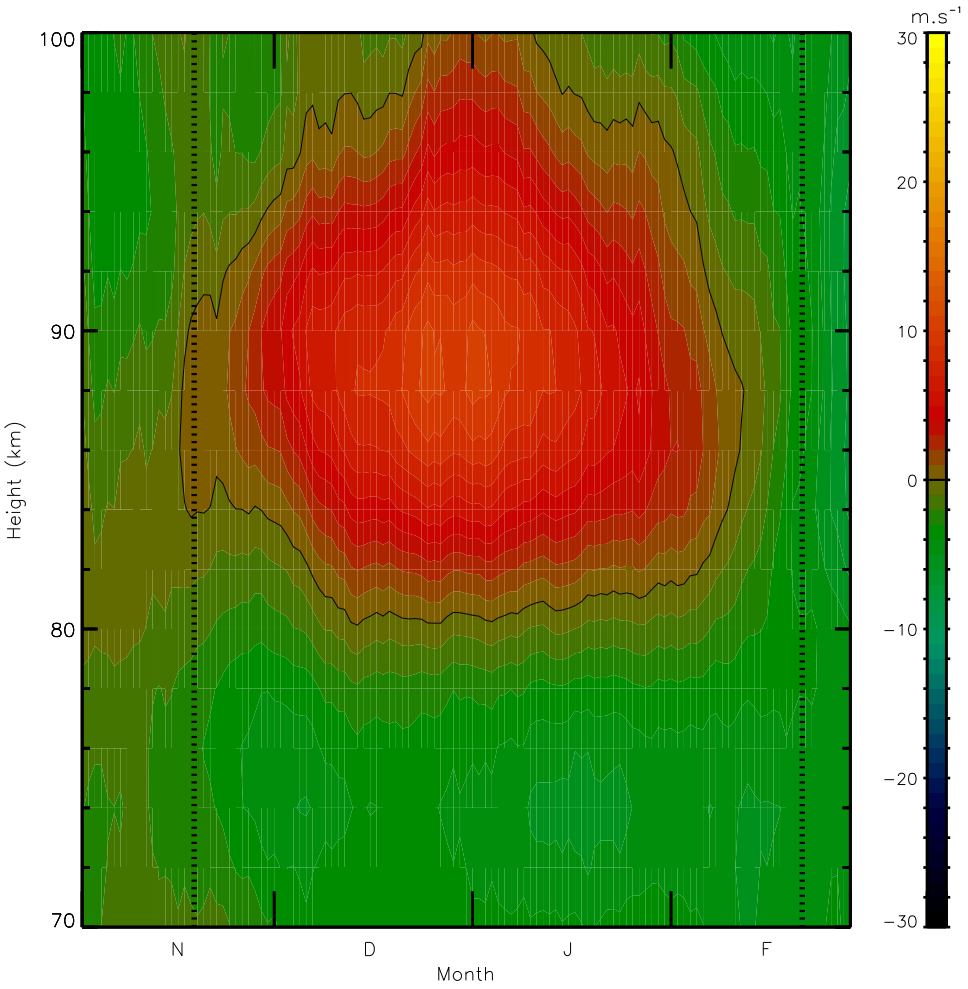

Figure 3.11: Meridional winds at Davis during summer (using the data shown in Figure 3.5). The dotted lines indicate the start and end of PMSE observations obtained from the Davis VHF radar during the 2003/2004 southern summer.